Improved Resonant Converters with a Novel Control Strategy for High-Voltage Pulsed Power Supplies

Dianbo Fu

Thesis submitted to the Faculty of the
Virginia Polytechnic Institute and State University
in partial fulfillment of the requirements for the degree of

Master of Science
in
Electrical Engineering

APPROVED:

Fred C. Lee, Chairman

Fei Wang

Yilu Liu

July 26, 2004
Blacksburg, Virginia

Key Words: Pulsed power supply, resonant converter, power factor, high power density

Improved Resonant Converters with a Novel Control Strategy for High-Voltage Pulsed Power Supplies

Abstract

By

Dianbo Fu

Committee Chairman: Dr. Fred C. Lee

Electrical and Computer Engineering

The growing demand for high voltage, compact pulsed power supplies has gained great attention. It requires power supplies with high power density, low profile and high efficiency. In this thesis, topologies and techniques are investigated to meet and exceed these challenges.

Non-isolation type topologies have been used for this application. Due to the high voltage stress of the output, non-isolation topologies will suffer severe loss problems. Extremely low switching frequency will lead to massive magnetic volume. For non-isolation topologies, PWM converters can achieve soft switching to increase switching frequency. However, for this application, due to the large voltage regulation range and

high voltage transformer nonidealities, it is difficult to optimize PWM converters. Secondary diode reverse recovery is another significant issue for PWM techniques.

Resonant converters can achieve ZCS or ZVS and result in very low switching loss, thus enabling power supplies to operate at high switching frequency. Furthermore, the PRC and LCC resonant converter can fully absorb the leakage inductance and parasitic capacitance. With a capacitive output filter, the secondary diode will achieve natural turn-off and overcome reverse recovery problems. With a three-level structure, low voltage MOSFETs can be applied for this application. Switching frequency is increased to 200 kHz.

In this paper, the power factor concept for resonant converters is proposed and analyzed. Based on this concept, a new methodology to measure the performance of resonant converters is presented. The optimal design guideline is provided.

A novel constant power factor control is proposed and studied. Based on this control scheme, the performance of the resonant converter will be improved significantly. Design trade-offs are analyzed and studied. The optimal design aiming to increase the power density is investigated. The parallel resonant converter is proven to be the optimum topology for this application. The power density of 31 W/inch^3 can be achieved by using the PRC topology with the constant power factor control.

Acknowledgements

I would like to express my deep and sincere appreciation to my advisor, Dr. Fred C. Lee for his guidance, encouragement and continuous support. He offered not only his professional expertise and mentoring; he also .taught me the correct attitude toward research, which can be applied to every aspect of my life as well.

I am very grateful to my master committee members: Dr. Fei Wang and Dr. Yilu Liu for their valuable suggestions and plentiful help.

I must thank all the members of the Center for Power Electronics Systems (CPES) for their friendship, support, discussion and encouragement. My study and research experience in CPES is enjoyable and rewarding. In particular, I should like to thank Dr. Ming Xu, Dr. Bo Yang, Dr. Wei Dong, Dr. Lingyin Zhao and Dr. Qun Zhao for leading me into the field of power electronics.

Special appreciation goes to Mr. Yang Qiu and Mr. Bing Lu, who helped me with my experiment and shared their research results and knowledge with me. Their assistance and encouragement were invaluable throughout this work.

I also wish to express my gratitude to my close friends Mr. Rengang Chen and Mr. Bryan Charboneau. Rengang helped me with my experiment and worked with me until

dawn on several days, which moved me. Bryan deserves very special gratitude for his continuous support, collaboration and encouragement.

I also extend my appreciation to Mrs. Qian Liu, Dr. Gang Chen, Mr. Liyu Yang, Mr. Yuancheng Ren, Mr. Jinghai Zhou, Mr. Jia Wei, Mr. Shuo Wang, Dr. Francisco Canales, Mr. Xigen Zhou, Mr. Chuanyun Wang, Mr. Yonghan Kang, Mr. Wei Sheng, Mr. Hongfang Wang, Mr. Chucheng Xiao, Mr. Xiangfei Ma, Mr. Chong Han, Mr. Bin Chen, Mrs. Ning Zhu, Miss Jinghong Guo and Miss Manjing Xie for their valuable suggestions, comments and discussions.

My heartfelt appreciation goes toward my great parents, Zhiyang Fu and Huizu Zhang. Their love, patience, sacrifice and encouragement for me are highly appreciated. Indeed, they were my major source of strength and support.

Finally, I would like to deeply thank my wife Peipei for her love, devotion and belief in me. She is the one who paid the greatest sacrifice to make me succeed. I am forever grateful for her endless support and love.

Table of Contents

List of Illustrations

List of Tables

Chapter 1

Introduction

1.1 Background and Objectives

Pulsed power is a broad technical field that is united by a common activity—the transformation of electrical energy into high-peak power pulses. The value in this activity is the effect pulsed power achieves in a variety of applications. For just a brief moment, pulsed power enables the generation of extremely high temperatures, brilliant flashes of light and powerful bursts of sound. It accelerates particles to great velocities, produces tremendous forces, detects objects at a great distance, and creates many other extreme conditions that are simply impossible to sustain continuously.

Pulsed power is an enabling technology that is often overlooked as a part of everyday life. In medicine, pulsed power drives the accelerator devices that generate X-ray treatments for millions of cancer patients worldwide. It provides the life-giving jolt in pacemakers and defibrillators, but also gives us the ability to visualize a developing fetus with gentle ultrasonic pulses. In industry, pulsed power drives the lasers that do the raw work of cutting and welding as well as the lasers that do the delicate work of semiconductor fabrication with intense ultraviolet radiation. Pulsed power is at work behind the scenes: from the miniature power supply in a laptop computer, to the motor

speed controls in a modern subway system, to the flash in our camera, pulsed power is the service technology that makes it all possible [A-1, A-2].

Recent world events have spotlighted the need for high voltage pulsed power systems in new applications. The need to treat mail contaminated with anthrax and the use of accelerators to produce high power X-rays for security screening are highly visible examples. High voltage pulses, both directly and as the front end of particle accelerators, enable multiple processes for killing microorganisms in food processing, medical equipment sterilization, and wastewater treatment. Development of faster microcircuits has driven significant research in the use of high voltage pulsed power systems for lithography and ion implanters for wafer fabrication. High Definition Television (HDTV) is driving a large-scale upgrade of broadcast transmitters. Each of these commercial applications requires high voltage pulsed power systems [A-4, A-5].

The recent advancements in new solid-state devices and high energy density components have enabled pulsed power systems to remain powerful, yet shrink in size and weight. Our thirst for reducing the size of overall products or systems with improved efficiency extends well beyond the general consumer market to include defense, industry, medicine and research. A growing demand for size and weight reduction of pulsed power systems has stimulated substantial development and research efforts in high power density, low-profile pulsed power supplies.

Typical durations of the single or repetitive power pulses are in the range between nanoseconds and seconds. Most pulsed power devices use capacitors to feed the

respective electric loads, via a high-power switch, with electrical energy. The capacitive energy is used to generate electric or magnetic fields. Electric fields can be used to accelerate charged particles leading in general to thermal, chemical, mechanical, electromagnetic-wave or break-down effects. Magnetic fields together with electric fields transfer energy as electromagnetic waves. X-ray, microwaves and laser beam generation are typical examples. Magnetic fields facilitate the generation of extremely high pressures in ranges of 0.1 GPa and more. These effects can be applied to remodel, compress, weld and segment materials as well as to modify the surface of organic and inorganic parts.

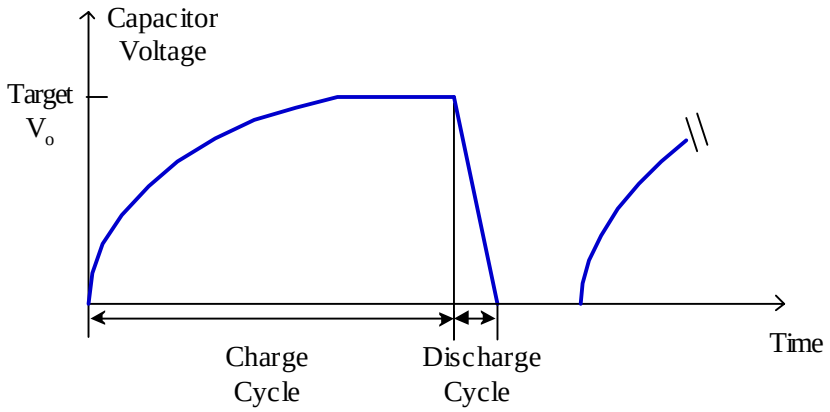

Fig. 1.1. The capacitor charging voltage

The short but intense bursts of energy required for pulsed power systems are often obtained by rapidly discharging an energy storage capacitor. These capacitors must be charged by a capacitor-charging power supply (CCPS) prior to releasing the stored energy to the load. Fig. 1.1 shows the voltage across the energy storage capacitor connected to the output of the CCPS. As seen in this figure, the capacitor voltage is

divided into two cycles: charging and discharge. During the discharge cycle, the CCPS is disabled while the capacitor is rapidly discharged by the load, which is inactive in the charge cycle. The discharge cycle is normally much shorter than the charge cycle. The CCPS enters the charge cycle with near short-circuit conditions across its output terminals and begins operation in the charging mode. In this mode, the CCPS operates at its maximum charging capability while charging the capacitor to the target voltage. The CCPS moves from the charging mode to the refresh mode when the target voltage is reached and remains in this mode until the load discharges the capacitor. The output voltage may drift due to capacitor leakage and output voltage sensing network. The CCPS compensates for any drift by supplying a small current to the energy storage capacitor. This current may be supplied continuously in a manner similar to trickle charging a battery or discontinuously in short bursts [A-7, A-8]. The refresh mode is important when the repetition rate, the frequency at which the load discharges the energy storage capacitor, is low.

In contrast to a conventional high-voltage DC power supply that delivers constant or near-constant power to its load, the output power of the CCPS varies over a wide range. The charging mode is characterized by high peak power. The instantaneous output power is almost zero at the beginning of the charging mode, and, if the charging current is constant, the peak instantaneous output power occurs at the end of the charging mode. The refresh mode is typically a low-power mode because the currents are small compared to those in the charging mode. The average output power for a CCPS

depends on the repetition rate and is at its maximum when the capacitor is discharged at the end of the charging mode.

Due to the high amount of energy per discharge, the load is often operated in a short burst mode. This allows operation of both the load and the rapid capacitor charger in so-called “Thermal Inertia” mode, meaning that the generated heat is absorbed by the thermal capacity of the circuit elements themselves. Operation in “Thermal Inertia” mode always means that cooling fins, plumbing, heat exchangers etc. can be eliminated. In some cases, circuit elements can also be overloaded. For example, current levels in power resistors and magnetic coils can significantly exceed rated levels for a few seconds. However, this is not true for currents in power semiconductors, where rated levels can typically only be exceeded for microseconds. Furthermore, exceeding flux levels in magnetic structures, which can lead to saturation will immediately limit their performance and is therefore not helpful in most cases.

1.2 Objective of This Study

The objective of this thesis is to develop designs of high voltage, high efficiency and high power density pulsed power supply for capacitor charger. The specifications of this pulsed power supply are list below:

Load capacitor:	400 μF
Input DC bus voltage:	600 V

Capacitor bank charging target voltage	10 kV
Charging time	8~10 S
Charging power during charging mode	>2kJ/S
System power density	>20 W/in^3
System efficiency of full power operation	>90%
System operation temperature	37 ^{o}C
System thermal management	Natural cooling

Capacitor charging operation scenarios:

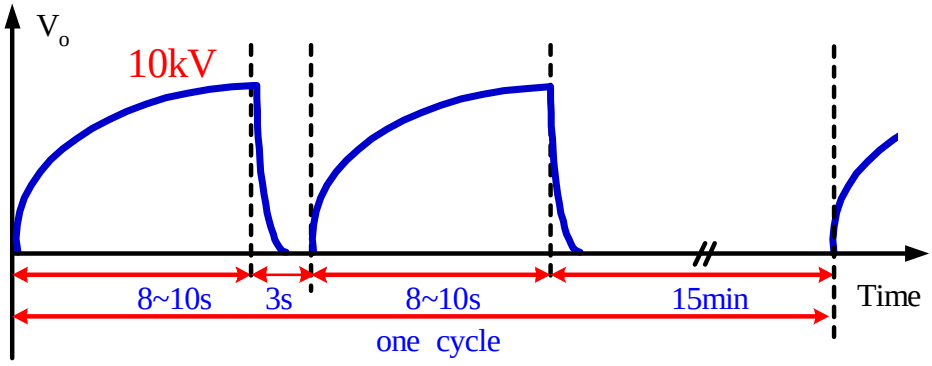

Fig. 1.2. Capacitor charging operation scenarios

The overall requirement of this pulsed power supply is much more stringent than the conventional CCPS. The high power density requirement is far beyond state-of-the-art technology and becomes the primary design criteria. In addition, the thermal condition of this pulsed power system is very severe due to high ambient temperature

and a non-cooling environment. Also, the high efficiency and high step-up voltage raise the design difficulty further. In short, the design of such high power density, high efficiency pulsed power supply is a very serious challenge and will involve circuit topologies investigation, high frequency operations, magnetic designs and system optimization.

1.3 Thesis Organization

This dissertation is divided into five chapters. They are organized as following.

The first chapter is the background review of pulsed power systems and capacitor-charging power supplies. Trends for this application are high-power density, high efficiency and low profile. To achieve high-power density, high switching frequency is a must. This calls for advanced technology. The primary target of this thesis is to develop technique to achieve high-voltage, high-efficiency, high-power-density pulsed power supplies that could be optimized under the stressed thermal environment while being able to provide the energy to the load capacitor very rapidly.

In Chapter 2, a set of topologies and characterization techniques for pulsed power systems are introduced. The state-of-the-art topologies for a capacitor-charging power supply are analyzed and compared. Extremely high voltage stress makes non-isolation topologies such as boost converters not suitable for this application. The conventional PWM technique will suffer from the high switching loss and therefore low switching frequency and large magnetic components volume. The operation with phase-shift

control allows the implementation of soft-switching techniques. However, the large turns ratio of the transformer will exacerbate the transformer nonidealities. These nonidealities will cause undesirable voltage and current spikes which can damage circuit components and greatly increase switching loss. Finally, the resonant converter has been analyzed and compared for this application. With the soft-switching technique and transformer parasitics utilization, the LLC and parallel resonant converter (PRC) are considered as good candidates to achieve the goal of high power density.

In Chapter 3, a novel developed power factor concept of resonant converters is addressed. Based on this concept, optimized designs of resonant converters are discussed. According to the analysis of resonant converter power factor, the optimal design guideline is provided.

Chapter 4 is dedicated to the investigation of optimal designs for capacitor-charging power supplies. A novel constant-power factor control scheme is proposed. With this control method, the system efficiency will be highly improved. LCC and PRC are both good candidates based on this new control method. Finally, PRC is chosen due to the less passive components volume and therefore higher power density. The power density of this CCPS will be 31 W/in^3, which may be among the highest power densities that have ever been reported before.

The conclusions and the suggestions for future work are given at the end of this thesis.

Chapter 2

Literature Survey on Topologies and Techniques for Pulsed Power Supplies

2.1 State-of-The-Art Topologies

2.1.1 Non-Isolated Topologies

As this pulsed power system does not require the isolation in the power flow, the use of a high voltage transformer will not be the first solution. Therefore, several non-isolated type topologies are discussed in this section.

The single boost converter has been reported to be applicable in this application [B-1]. According to the system specifications, the converter needs to step up the 600 V input voltage to 10 kV target voltage. The DC voltage gain will exceed 16. In order to provide such a large DC gain, a normal boost converter would have to operate at a pretty high steady state duty cycle—larger than 94%. Operation at high switching frequency would be impossible, due to the fact that the diode does not turn on or turn off instantaneously. The switching times will take all the diode conduction time. For compensating changes in load or line, the duty cycle may have to be increased, and a serious latch-up operation appears [B-2, B-3]. An extremely high duty cycle is also not

desirable owing to diode reverse recovery problems: the diode would conduct for a very short time period, and the high diode forward current and output voltage would degrade the efficiency. The circuit is limited to around several kHz due to the switching loss in the power devices. As a result the boost inductor becomes bulky and leads to low power density.

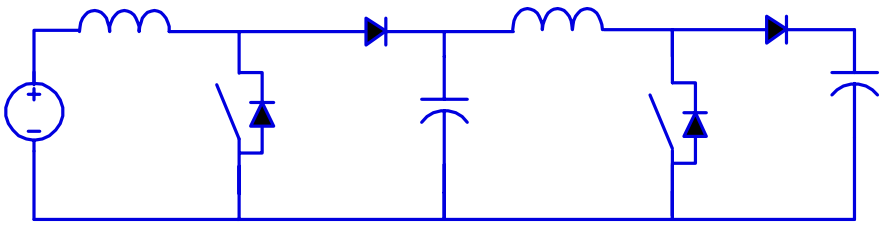

Fig. 2.1. The cascaded boost converter

A cascade of two DC/DC boost converters has been proposed in [B-4], where an intermediate DC voltage is established between the two stages. As seen in Fig. 2.1, by applying this structure, the high duty cycle problem can be solved. However, this cascade of two boost converters implies a low total efficiency, which is equal to the product of the efficiencies of each converter. Furthermore, the high voltage stress (10 kV) on power devices of the second boost converter still remains. At high voltage levels, excessive series of switch elements such as MOSFETs or IGBTs to share high voltage stress becomes physically cumbersome and impractical, while SCRs or GTOs limit the operating frequency and result in lower efficiency, greater switch drive requirements and large magnetic volume.

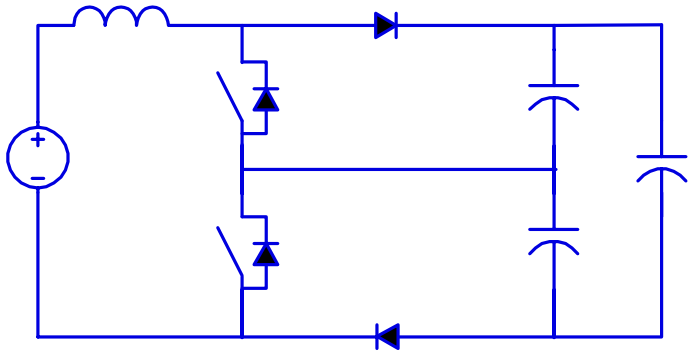

Fig. 2.2. The three-level boost converter

Another non-isolated step-up topology is the multilevel boost converter. The three-level boost converter, which is shown in Fig. 2.2, has been widely investigated in Power Factor Correction (PFC) application [B-5, B-6, B-7]. By using the three-level boost topology in the high-voltage applications, some advantages can be achieved over the usual boost converter. With the three-level boost converter, the inductance of the boost inductor can be reduced, and the semiconductor devices' voltage rating is half of the output voltage. Therefore, the converter power density and efficiency will be improved. As can be seen, even though the voltage stress across the power devices has been reduced to half of the output voltage, it is still difficult to apply the fast switching devices such as MOSFETs and IGBTs.

In order to reduce the voltage stress of the semiconductor devices, further development of three-level boost converter will lead to a higher multilevel boost converter, which is proposed here and depicted in Fig. 2.3. It should be noted that when the number of levels is beyond four, bidirectional voltage-blocking devices have to be

used. In Fig. 2.3, two combined IGBT constitute such a bidirectional voltage-blocking device.

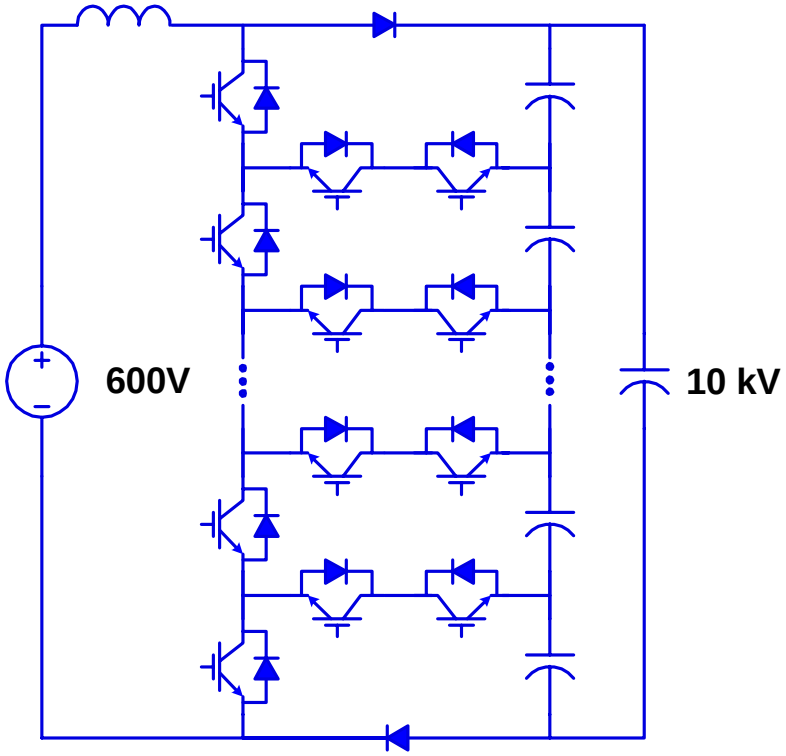

Fig. 2.3. The high multilevel boost converter

If N-level (N>4) boost converter is used, the voltage stress on an active switch will reduced to 1/(N-1) of output voltage. Therefore, a high switching IGBT device can be applied. More important, the frequency of boost inductor will increase to N-1 times of the device switching frequency. This will result in smaller magnetic volume. However, the drawback of this kind of topology is obvious. This converter requires a high number of switching devices. The bank of series capacitors' voltage balancing is another serious issue. Also, these series capacitors are energy storage components. Therefore, large size of these capacitors is inevitable.

According to above discussion, a conclusion may be drawn here that the non-isolated type topologies are not a good fit for this stringent space application due to high voltage stress and a large volume of passive components.

2.1.2 High Voltage Transformer Model

For the isolated type topology, a transformer is always necessary. In this section, a simplified high-voltage transformer model is given.

Power transformers designed for high-voltage applications contain parasitic reactances that are generally much larger than those of their low-voltage counterparts. The leakage inductances and the reflected distributed capacitance are large due to the following reasons. When a high-voltage transformer is employed, it requires a relatively large space between the primary and secondary windings due to the insulation requirement. This leads to relatively large leakage inductance. The distributed capacitance is the total lumped capacitance that is associated with the windings. In a high-voltage transformer, the secondary layer-to-layer and terminal capacitances are the major contributors to this total. The effect of parasitics associated with the transformer becomes accentuated as the secondary to primary turns ratio is increased.

Fig. 2.4 illustrates the equivalent circuit of a high-voltage transformer. In Fig. 2.4, L1 and L2 are leakage inductance, R1 and R2 are resistances related with winding losses, C1 and C2 are intra-winding self-capacitances, and C12 is mutual capacitance between primary and secondary windings. L_m is the magnetizing inductance and R_{core} is the resistance corresponding to core losses.

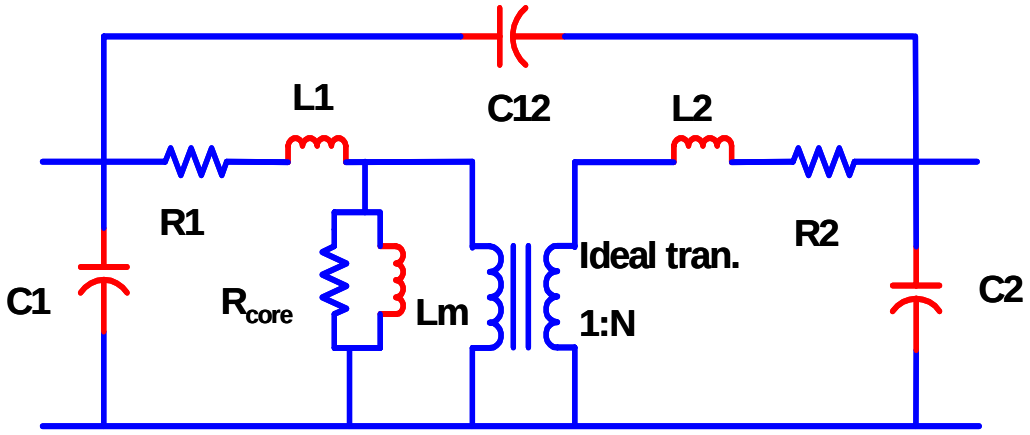

Fig. 2.4. The equivalent circuit of high voltage transformer

In the transformer inductances, magnetizing inductance L_m can be considered negligible because it is in parallel with the primary windings and is much greater than other inductances. If the magnetizing inductance is neglected, leakage inductance can be treated as the lumped leakage inductance L_k of the transformer when reducing secondary leakage inductance into primary. In aforementioned capacitances, C12 can be neglected because it is much smaller than the others. In particular, when secondary to primary turns ratio is very high, C1 is small enough to be neglected as compared with C2 which is reduced to the primary side by factor N2. Therefore, C2 is considered as the dominant winding capacitance Cs of the high-voltage transformer.

As discussed above, a lumped-element high-voltage transformer circuit model is expressed in terms of the leakage inductance L_k, the winding capacitance C_s, and the ideal transformer with the turns ration N. The model is shown in Fig. 2.5.

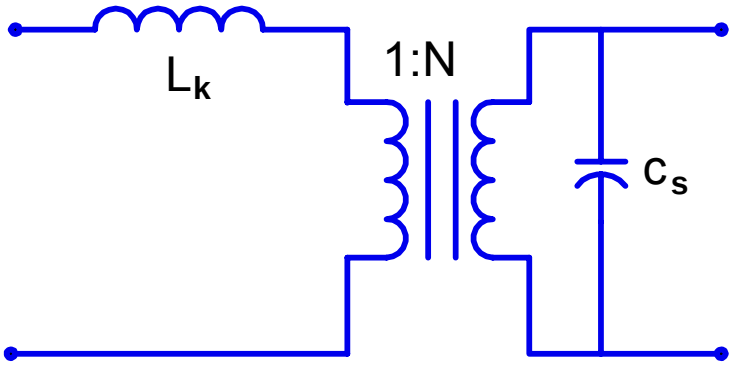

Fig. 2.5.A lumped-element high-voltage transformer circuit model

2.1.3 PWM Converter

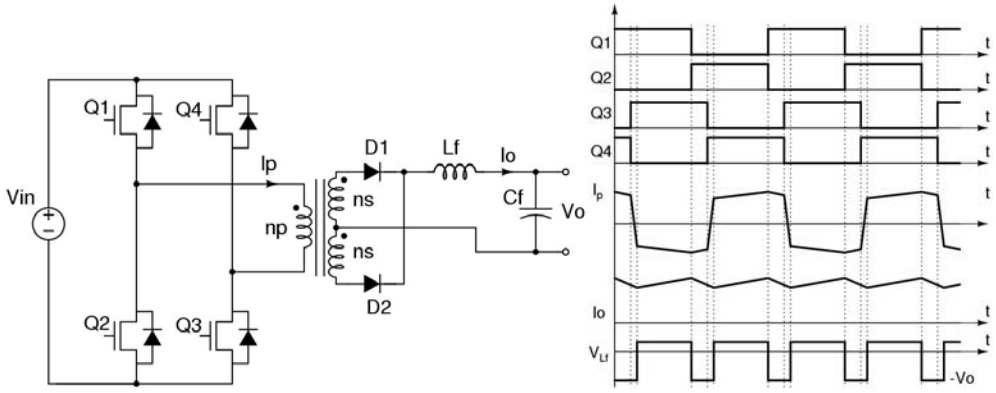

Fig. 2.6. Phase-shift full-bridge converter and operating waveforms

The full bridge (buck-derived) DC/DC converter with isolation on the intermediate high frequency AC link is a very popular topology in many applications. The main advantages of this topology include constant frequency operation which allows optimal design of the magnetic filter components, pulse width modulation (PWM) control, minimum voltage current stresses and good control range and controllability. However, the increase in device switching losses as the frequency increases and the high voltage

stress induced by the parasitic inductances following diode reverse recovery are major drawbacks of this topology.

Various soft-switching schemes (ZVS and ZCS) have been proposed to improve the performance of hard switching PWM converters. One of the most popular topologies is the phase shift full bridge converter, which is illustrated in Fig. 2.6 [B-8, B-9, B-10, B-11, B-12]. In this topology, the transformer leakage inductance and the device's output capacitance are effectively utilized to achieve zero voltage switching (ZVS). The load range can be extended by properly sizing the leakage inductance of the transformer. In [B-16, B-17], capacitor-charging power supplies were implemented by this PWM technique. However, there are several disadvantages of this topology. To assure ZVS in a wide range of loads, it is necessary to have sufficient stored energy in the leakage inductor. Especially at light loads, the energy stored in the leakage inductor of the transformer is not sufficient to achieve ZVS. Therefore, there is a need of adding another external inductor in series with the primary winding of the load, where ZVS can be maintained. A large commutating inductor enables ZVS in wide range of loads but also causes higher circulating energy. It will increase the conduction loss. The smaller the duty cycle, the more circulating energy there is. In the capacitor-charging power supply, it is expected that the load and output voltage will be variable. Therefore, the duty cycle range will be 0% - nearly 50%. This will increase circulating energy. Secondary-diode reverse recovery is another significant problem in PWM converters. These high-voltage diodes are located between the leakage inductance of the transformer and the output filter inductance. Hence, they serve as switches connecting

two current source elements and experience very high stresses. Excessive voltage overshoots occur when the secondary diodes snap off. Higher output voltages require higher voltage diodes that have very poor recovery characteristics which exacerbate the problem. If softer, lower voltage diodes are used in series, a very lossy voltage-sharing circuit is required. Usually, a resistor-capacitor-diode (RCD) arrangement is used to clamp the voltage overshoot and dissipate the recovery energy. If the converter operation demands a significant variation in duty cycle, the clamp design cannot be well optimized, leading to higher losses. Alternative techniques have involved the use of an active or passive secondary side clamp [B-13, B-14, B-15]. However, due to the high voltage stress and variation of operation conditions, very few clamp circuits are favorable for this application.

Because of these disadvantages of PWM converters, high power density CCPS can not be achieved by applying PWM topologies.

2.1.4 Resonant Converters

In the previous section, the high voltage transformer model was derived. The leakage inductance and the stray capacitance can significantly change converter behavior. The former causes undesirable voltage spikes which can damage circuit components, and the latter results in a current spike and slow rise time. An attractive alternative for high-voltage DC-DC applications is the use of the resonant converter in which the transformer parasitics can be incorporated into the basic operation of the circuit. We could utilize the leakage inductance and parasitic capacitance partially or

wholly as resonant tank elements, and thereby turn these nonidealities into useful articles.

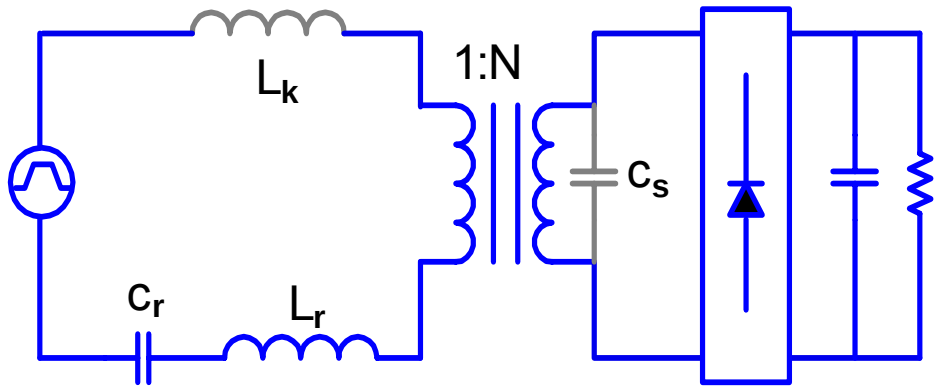

Fig. 2.7. The SRC with transformer equivalent circuit included

The series resonant converter (SRC) has been widely used in CCPS [B-18]-[B-21]. It can achieve ZCS or ZVS and lead to very low switching loss thus enabling CCPS to operate at a high switching frequency. A simplified SRC with transformer parasitics is shown in Fig. 2.7. As this figure shows, the transformer leakage inductance L_k is integrated into the power topology because it contributes to the resonant inductance L_r. However, the parasitic capacitance C_s is not placed in parallel with the resonant capacitor C_r, and thereby can not be absorbed by the resonant converter. The winding capacitance adds an additional element to this tank circuit which prevents the output rectifiers from switching instantly. As a result, an additional subinterval is created during which the winding parasitic capacitance is charged from positive peak voltage to negative one or vice-versa. During this time, all four output diodes are reverse-biased and no charge is transferred to the output. Therefore, the output voltage is reduced somewhat from the ideal series resonant converter case, while the tank and switch

current are increased. This effect has been quantified in [C-1]. Another drawback of SRC is that the frequency band to achieve output voltage regulation over an appreciable range of loads will be very large. Therefore, optimization of the converter is very difficult.

Though it cannot utilize the transformer parasitic capacitance, SRC is still applied to the application of pulsed power systems. If another resonant topology could absorb both parasitic inductance and stray capacitance, it would be the optimum topology for the high voltage capacitor-charging power supply.

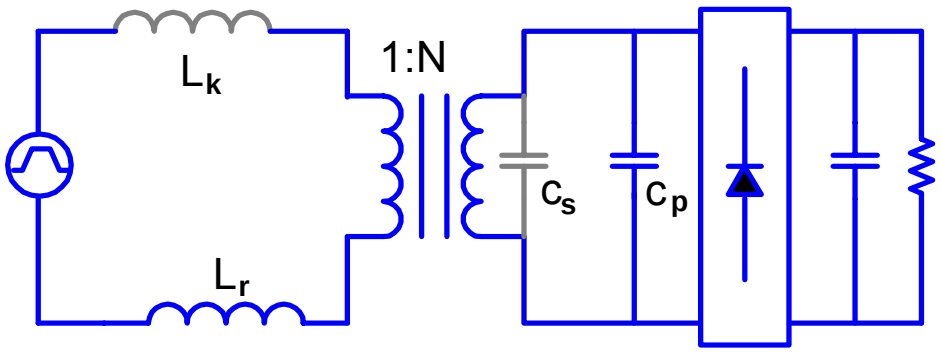

Fig. 2.8. The PRC with transformer equivalent circuit included

The Parallel Resonant Converter (PRC) overcomes the drawbacks of the SRC. A high-voltage version of the PRC with no output filter inductor is represented in Fig. 2.8. Note that the resonant capacitor C_p has been moved to the transformer secondarily. Therefore, the parasitic capacitor of the transformer appears directly in parallel with the resonant capacitor. Meanwhile, the transformer leakage inductance appears in series with the resonant inductor. Consequently, the PRC topology can integrate the high-

voltage transformer parasitics very well and transformer nonidealities do not degrade operation of the converter.

Another promising topology is the LCC or series parallel resonant converter shown in Fig. 2.9. Similar to PRC topology, LLC can fully absorb the transformer parasitics. Furthermore, with an additional resonant element, LLC exhibits better control characteristics than the conventional two elements resonant converters. It is also shown that, by a proper choice of operating point, transformer winding capacitance can completely replace the external discrete resonant capacitor and the leakage inductance can add to the external resonant inductor. As a result, depending on the topology used, the transformer nonidealities can become an asset rather than a liability.

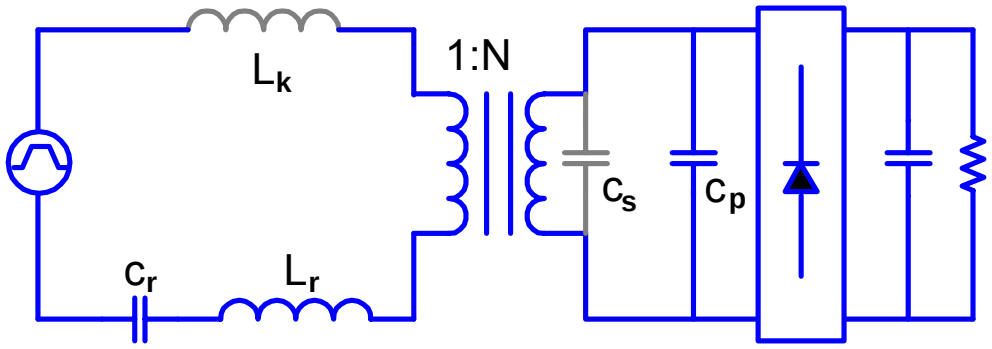

Fig. 2.9. The LLC with transformer equivalent circuit included

In short, both PRC and LCC resonant converters can provide soft switching and avoid the reduction of efficiency with the increment of the switching frequency. The high switching frequency can effectively reduce the reactive elements such as inductors, capacitors and the high-voltage transformer. The transformer parasitics like leakage inductance and stray capacitance can be fully utilized by PRC and LCC converters.

These converters also show good voltage regulation and operation with a large variation of the load. Based on the above topology analysis, the PRC and LCC have been considered as good candidates in high voltage DC-DC converter design.

2.2 Pulsed Power Supplies with High Power Density

2.2.1 Introduction

In the Center for Power Electronics Systems (CPES), 2004, Yang Qiu and Bing Lu proposed a high frequency three-level LCC converter for high-voltage capacitor-charging power supplies. Their specification is almost same as the one described in previous chapter. The charging power rate is 2.6 kJ/S. The power density of the converter is 25 W/in^3, which is among the highest power densities that have ever been reported. The topology and the control schemes of this converter are briefly discussed in this section.

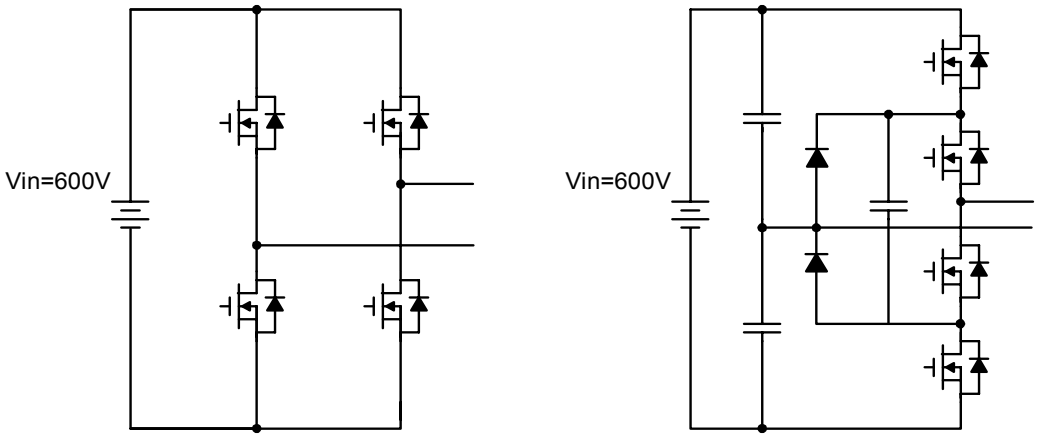

(a) Full bridge structure (b) Three-level structure

Fig. 2.10. Primary side structure comparisons

2.2.2 Topology Description

At these power levels, it is recommended to use a full bridge structure in the primary side as shown in Fig. 2.10. (a). In this case, each switch in the full bridge structure topology is subjected to the full bus voltage. In this voltage range, MOSFET devices with a high R_{dson} may be used. This approach may increase the conduction loss. Another option for this power range is to use IGBT devices. However, in this case the switching frequency, and consequently the power density of the converter, must be reduced. One way to reduce the voltage stress in the main devices and keep the requirements of high power operation is by using three-level structures as shown in Fig. 2.10 (b) [B-22, B-23, B-24]. In this kind of structure, the voltage stress across the power switch is reduced to half of the input voltage without increasing both the complexity and operation of the converter. In this way, lower voltage devices, which present better electrical characteristics, can be used.

Table 2-1. Main characteristics for the primary side of the load converter.

Structure	Device	Rating	R_{dson} (Ω)	Q_{gd} (nC)	FOM (Ω∗nC)
Full Bridge	APT12040L2FLL	1200V 30A	0.40	179	71.6
Three-level	APT6013LFLL	600V 43A	0.13	58	7.54

Table 2-1 presents the main characteristics of two devices that can be used for each structure for this application. As can be seen, the use of a three-level structure for the primary side will provide a significant improvement in efficiency at higher switching frequencies. Typically, the industry benchmark figure-of-merit (FOM) product R_{dson}*Q_{gd} is used here to represent the performance of different devices [B-25, B-26, B-27]. It is obvious that the FOM of 600 V MOSFET is much lower than 1200 V MOSFET. Therefore, 600 V MOSFET is preferred for this application. Taking into account these results, the three-level structure also becomes an interesting option when higher switching frequencies are required to increase the power density of the load converter.

The 10kV output is generated with the use of a three-level converter and a step-up transformer to convert the 600V input to 10 kV output. One single secondary can be used to generate the 20kV peak-to-peak waveform at a sufficiently high switching frequency. This method, although possible to implement, has a large voltage stress as a result of the large secondary voltage. Depending upon the type of insulation system that is used (epoxy, oil, air, etc.), the long-term reliability will be reduced due to the corona. Large reflected capacitances, due to the turns ratio (>1:12) will also limit the maximum switching frequency of the converter. Lower secondary AC voltages are desired in order to reduce the voltage stress on the insulation system. Four high-voltage secondary windings (approximately 2500 V zero to peak each) can be rectified, filtered and stacked in series to charge the 400 μF capacitor.

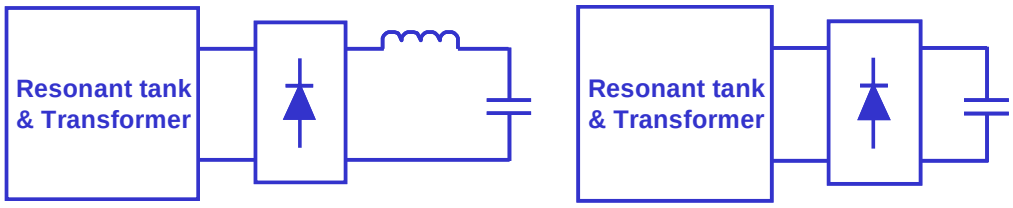

(a) Inductive filter. (b) Capacitive filter.

Fig. 2.11. Output filters for resonant converters

Another aspect of the circuit structure is the choice of the output filter. With an inductive or a capacitive output filter, which is shown in Fig. 2.11, the resonant converter will have different performances. With an inductive filter, the converter is able to achieve smaller output current ripple. However, with a capacitive filter, the bridge diodes are able to realize natural turn-off, as demonstrated in Fig. 2.12, therefore the reverse recovery stress is reduced. In this high-voltage application, the diode reverse recovery is a stringent issue. In addition, the high voltage inductor is saved with a capacitive filter. High voltage drop on this inductor is also avoided Size could be reduced. Consequently, the capacitive filter is adopted.

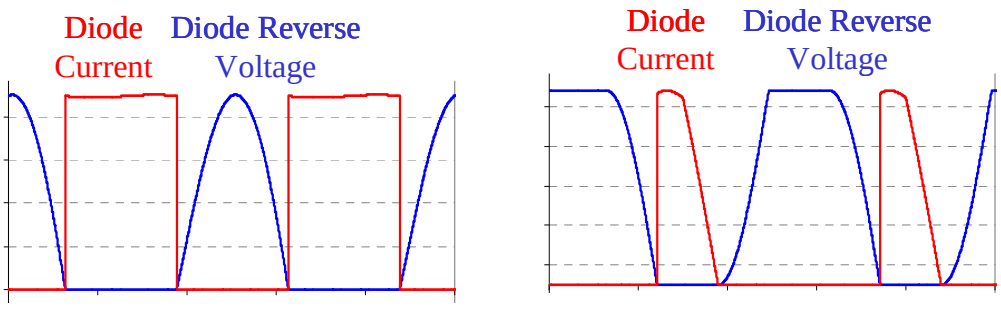

(a) Inductive filter waveform (b) Capacitive filter waveform

Fig. 2.12 Voltage and current waveforms on bridge diodes with different output filters

According to the above discussion, the topology of the resonant converter is shown in Fig. 2.13. A three-level structure is placed in the primary side in order to reduce the voltage stress across the primary switches, allowing the use of devices with better characteristics. A LCC resonant tank is used to absorb the transformer parasitic components and to provide ZVS operation for the primary switches. At the secondary side, four high-voltage secondary windings can be rectified, filtered and stacked in series to charge the load capacitor. Relatively low voltage rating diodes can be used. These diodes naturally commute during operation, resulting in a small reverse recovery issue. In addition, variation of the switching frequency is used to control the resonant tank current, output current, and therefore, the charging rate of the load capacitor.

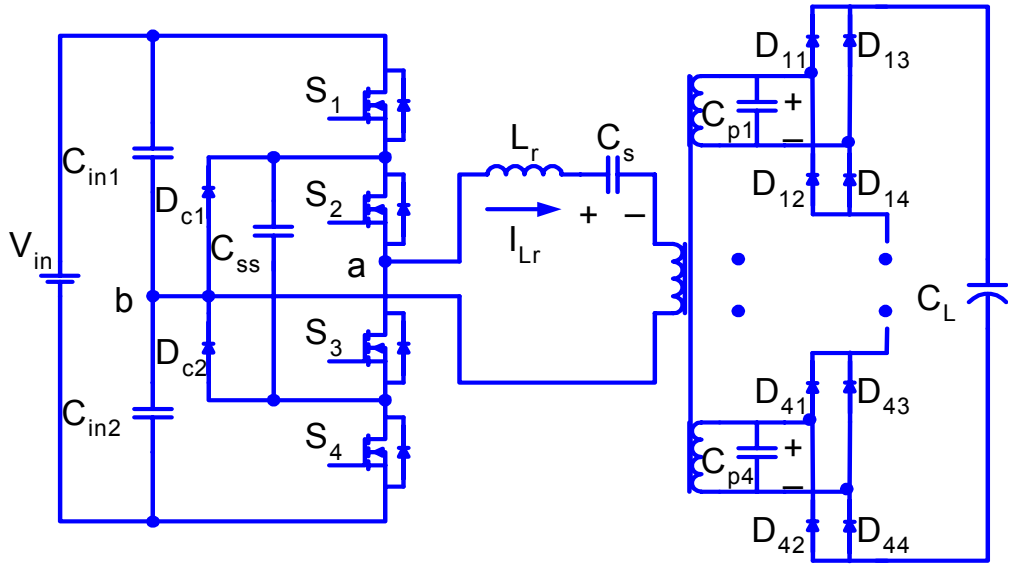

Fig. 2.13. The resonant converter topology for pulsed power supply

2.2.3 Control Analysis

The most common capacitor charging techniques are i) constant current and ii) constant power [C-31]. The constant current charging method provides a constant current during the charge period. The selection of the constant-charge current is determined by the required time.

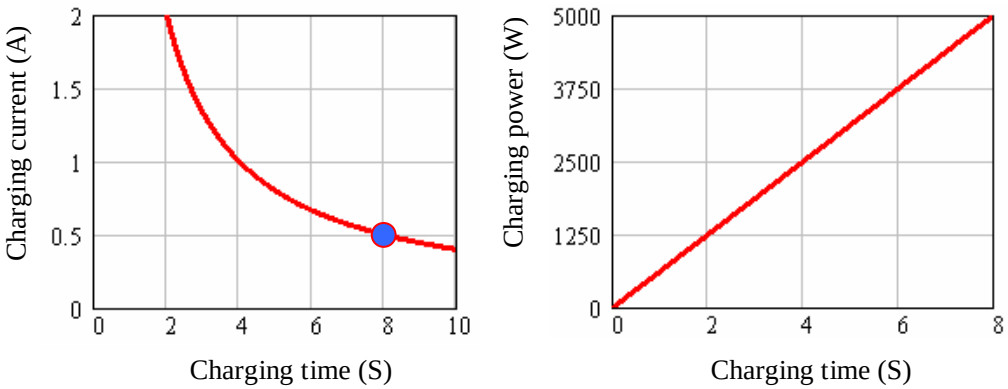

(a) Required constant charging current as a function of the charging time

(b) Output power as a function of the charging time for a 0.5A constant current charge

Fig. 2.14. Constant current charging method characteristics

Fig. 2.14 (a) shows the necessary constant current to charge the load as a function of the charging time. As can be seen in the graphs, to charge the equivalent capacitance of 400 μF within 8 seconds, it is necessary to select a constant current charge higher than 0.5 A. One of the problems that this method of charging presents is that at the end of the charge period, the output peak power of the converter exceeds the 5000 W as shown in Fig. 2.14 (b). This peak power imposes extra stress to the converter.

Constant-output power charge is another possible method to charge the equivalent capacitance without exceeding the output peak power. In this way, by changing the

output current as a function of the output voltage, it is guaranteed that during the charge process the peak power never exceeds the capabilities for the high-voltage converter. Considering a 2500 W constant-output power charge, the time to charge the equivalent capacitor will be 8 S. As shown in Fig. 2.15 (b), one of the disadvantages for this charging mode is that at a low output voltage the charge current will be very high.

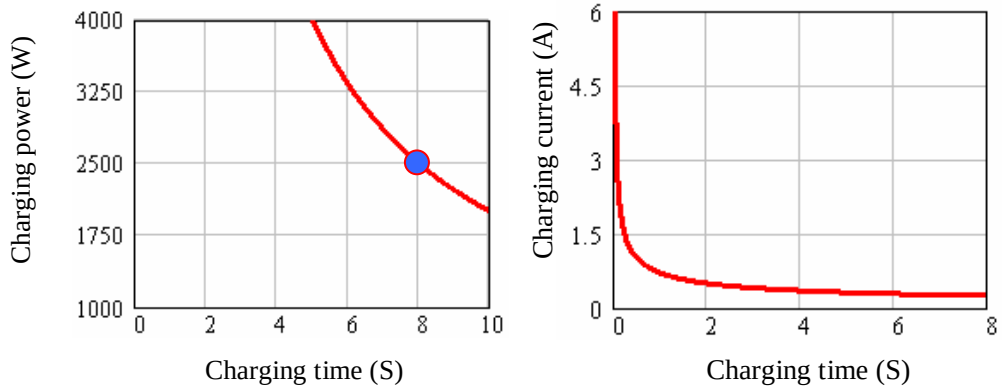

(a) Required constant charging power as a function of the charging time

(b) Output current as a function of the charging time for the 2500 W constant power charge

Fig. 2.15. Constant power charging method characteristics

In order to overcome the problems presented by these two methods of charge, Yang Qiu and Bing Lu proposed a hybrid charge method for this application. The main idea is to start the charge process using a constant-current charge mode. In this way, the current stress in the primary and secondary devices is limited. When the output power reaches the allowed output peak power, the process of charge is changed from a constant current charge to a constant power charge. The initial constant charging current will be set as 0.75 A. The constant charging power will be 3000 W. The load capacitor charging time will be 7.73 S. The power density of 25 W/in^3 is achieved

Chapter 3

Power Factor of Resonant Converters

3.1 Introduction

Resonant converters have become very attractive for power conversion, due to numerous advantages such as elimination of switching loss, low switching transients, reduced EMI and small size. However, most of the resonant converters developed so far include some inherent problems which have to be solved, such as reduced power conversion efficiency due to circulating energy generation. In order to increase the performance of resonant converters, it is necessary to reduce the circulating energy and improve the power conversion efficiency. In this chapter, the circulation energy or reactive power of resonant converters will be evaluated.

In general, the current and voltage of the primary side in isolated PWM converters are square wave and without a noticeable phase shift, as shown in Fig. 3.1. Therefore, virtually no circulating energy is generated during the power processing.

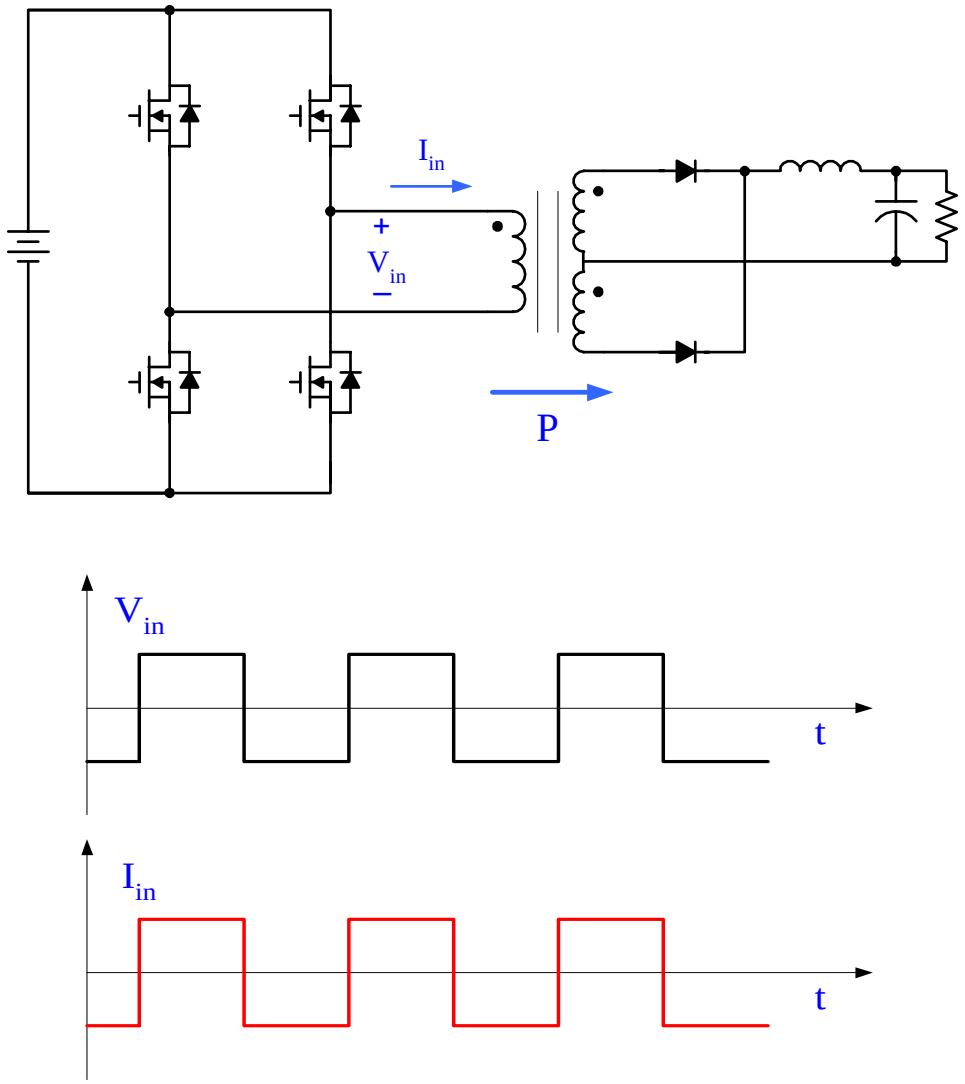

Fig. 3.1. Power processing in PWM converters

For the resonant converter, a square-wave inverter and a resonant network transfers and controls the fundamental power to the output in a piece-wise sinusoidal manner. As a result, the input voltage and current of the resonant tank exhibit a phase shift, which leads to circulating energy as shown in Fig. 3.2. The typical LCC resonant converter with inductive filter is exhibited in Fig. 3.2. Generally speaking, the amount of power

processed by the resonant converter is usually larger than that of a PWM counterpart with the same output power. This has an adverse effect on the performance of resonant converters. With the increment of circulating energy, the current stress of devices and resonant tank will increase. Therefore, the device loss and resonant tank size will be larger.

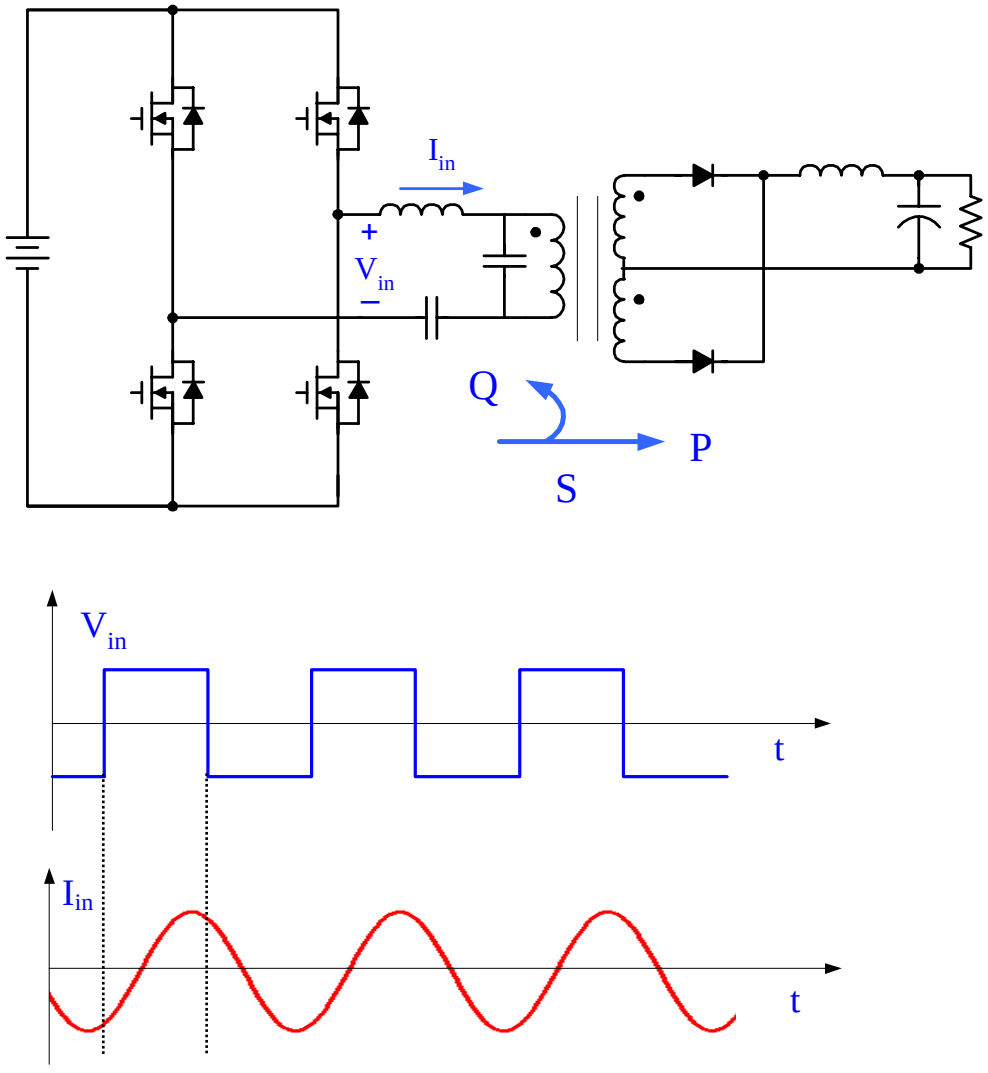

Fig. 3.2. Power processing of resonant converters

From the above discussion, it can be seen that a methodology to measure the effectiveness of power conversion is very important. It can help to optimize the resonant converter design with minimizing the circulating energy.

3.2 Analysis of Reactive Power and Power Factor

The rms value of the supply current $i(\omega t)$ that is mathematically continuous and periodic in T_c is given by: $I_{rms} = \sqrt{\frac{1}{T_c} \cdot \int_0^{T_c} i^2(\omega t) d\omega t}$

Similarly, the rms value of the supply voltage $v(\omega t)$ that is mathematically continuous and periodic in T_c is given by: $V_{rms} = \sqrt{\frac{1}{T_c} \cdot \int_0^{T_c} v^2(\omega t) d\omega t}$

The real or average power of the supply can be given by:

$$P = \frac{1}{T_c} \cdot \int_0^{T_c} v(\omega t) \cdot i(\omega t) d\omega t$$

The apparent power or apparent voltampers can be given by:

$$S = V_{rms} \cdot I_{rms}$$

The reactive power or circulating energy of the supply can be given by:

$$Q = \sqrt{S^2 - P^2}$$

The power factor is a figure of merit that measures how effectively energy is transmitted between a source and load network. It is defined as the ratio of the average power (or real power) entering the circuit to the product of root mean square (rms) voltage and rms current at the circuit terminals (or apparent power) [C-27, C-28, C-29]. Using the symbols defined above, the power factor can be written as:

$$PF = \frac{P}{S} = \frac{P}{V_{rms} \cdot I_{rms}}$$

It should be noted that the definition of the power factor is independent of current or voltage waveforms because P, V_{rms} and I_{rms} are all independent of waveform. Also, the equations expressed above can be derived by Fourier series analysis. The power factor always has a value between zero and one. The ideal case, unity power factor, occurs when the voltage and current waveforms have the same shape, contain the same harmonics and are in phase. For a given average power throughout, the rms current and voltage are minimized at the unity power factor.

3.3 Optimal Design to Reduce Reactive Power

The power factor of resonant converter is defined as the ratio of the output load power to the product of the rms voltage and rms current at the input of the resonant tank [C-30], as shown in Fig. 3.3. In this work, the described approach is extended to calculate the power factor of the resonant converter. A new methodology will be

proposed to evaluate the performance of the resonant converter and provide guidelines to optimize the design with the concept of power factor.

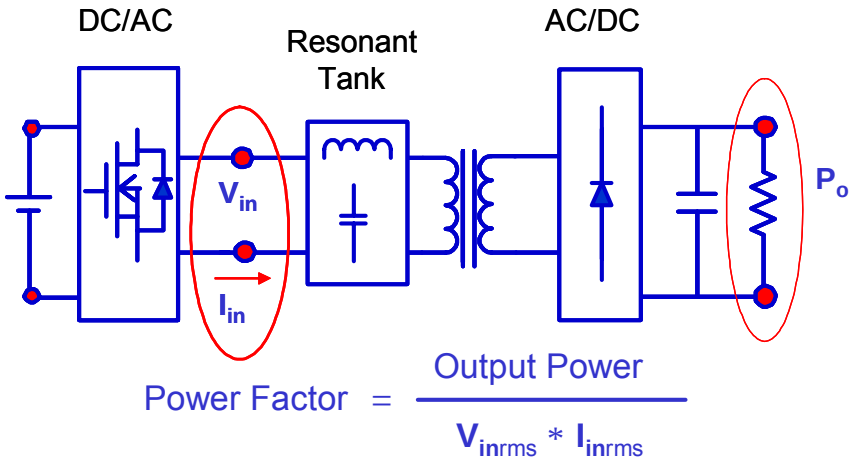

Fig. 3.3. The power factor of resonant converter

The major expressions of the resonant converter are represented below. For the sake of simplicity, the rms voltage and current at the input of the resonant tank are expressed as V_{in} and I_{in} respectively. I_o is the average output current.

Normalized voltage gain: $$M = \frac{V_o}{V_{in} \cdot n}$$

Normalized resonant current: $$I_N = \frac{I_{in}}{V_{in} / Z_o}$$

Normalized output current: $$I_{o\_N} = \frac{I_o \cdot n}{V_{in} / Z_o}$$

Normalized power: $$P_{o\_N} = \frac{P_o}{V_{in}^2 / Z_o} = \frac{V_o^2 / R_o}{V_{in}^2 / Z_o} = \frac{M^2}{Q_L}$$

Power Factor: $$PF = \frac{P_o}{V_{in} \cdot I_{in}} = \frac{P_o}{V_{in}^2 / Z_o} \cdot \frac{V_{in} / Z_o}{I_{in}} = \frac{P_{o\_N}}{I_N}$$

Corner frequency: $$f_o = \frac{1}{2\pi} \cdot \sqrt{\frac{1}{L_r \cdot \frac{C_r \cdot C_p}{C_r + C_p}}}$$

The resonant converter power factor can be expressed as the ratio of normalized resonant current to normalized power. Because the power factor can be described by the normalized parameters, it is very convenient to apply this concept to analyze and design the resonant converter.

The power factor curves of the LCC resonant converter are illustrated in Fig. 3.4. Seen from this figure, there are some remarkable characteristics. First, the maximum power factor is obtained when the converter operates at the resonant frequency. The resonant frequency f_r is defined as the frequency at which the phase shift of the voltage and current is equal to zero. The resonant frequency is different from the corner frequency or undamped natural frequency f_o. Secondly, the maximum achievable power factor of the resonant converter is around 0.91. Namely, the power factor of the resonant converter can not reach unit value. The power transfer from input to source is primarily via the fundamental component of the switching frequency. The harmonics of the source and load contribute little to the power transfer. Therefore, though voltage and current are in phase, the harmonics of voltage can not contribute much to the power conversion. In Fig. 3.5, Fourier series analysis shows that the rms value of the

fundamental component of V_{in} is about 0.9 times the rms value of the total harmonics, which implies a good agreement with the above discussion.

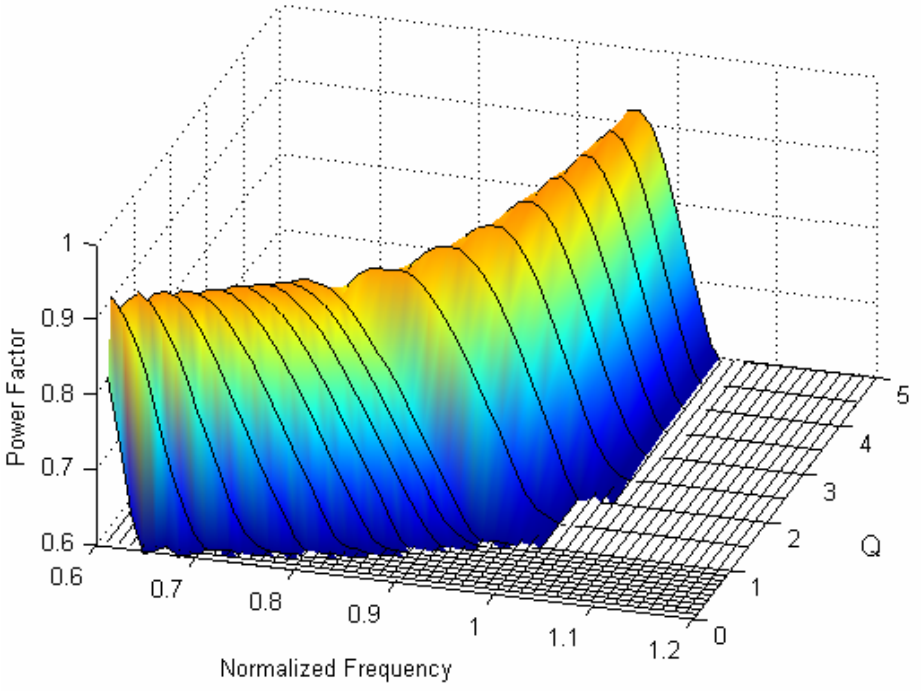

Fig. 3.4. 3-D power factor curves of LCC resonant converter versus f_s/f_o and Q

Fourier series analysis of V_{in}

$$v_{in}(\omega_s t) = \frac{4}{\pi} \cdot V_{in} \cdot \sum_{n=1,3\cdots}^{\infty} \frac{\sin(n\omega_s t)}{n}$$

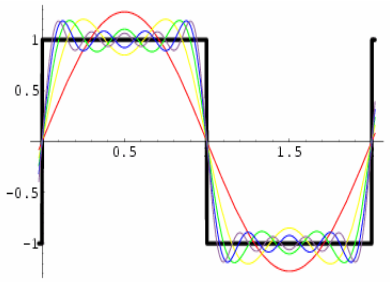

Fig. 3.5. The fourier series analysis of V_{in}

Further analysis shows that the power factor of the resonant converter is a good indicator to represent the efficiency of the resonant tank. The higher the power factor, the higher the system efficiency.

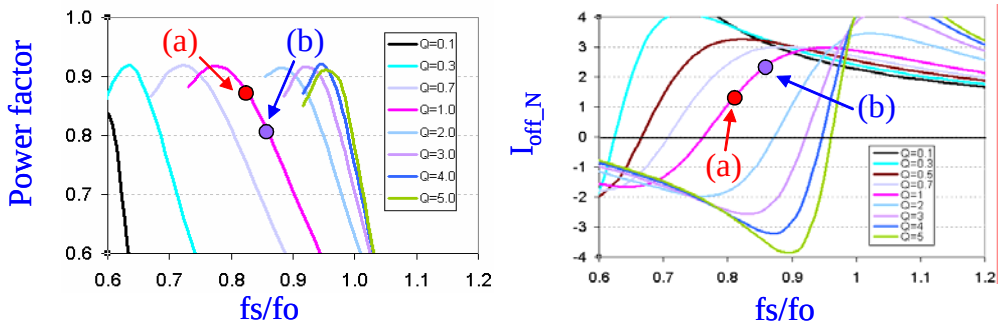

Fig. 3.6. Power factor curves and normalized turn off current curves

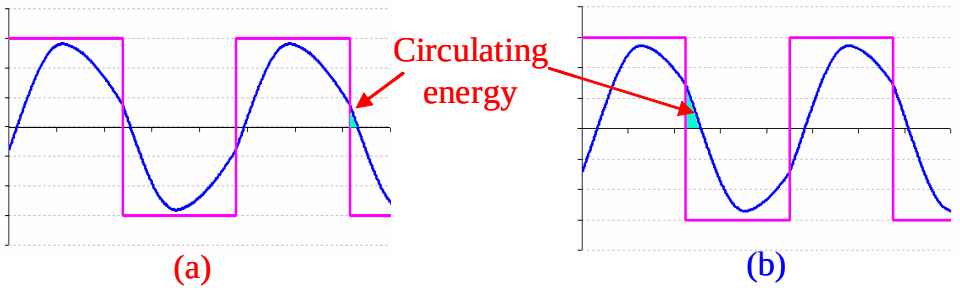

Fig. 3.7. The circulating energy of different operation points

With the same Q_L, at operating point (a), the converter is working close to the resonant frequency and has a relatively high power factor. As operating frequency increases, at operating point (b), the converter is working far away from the resonant frequency and the power factor becomes low, which can be observed from Fig. 3.6. From simulation waveforms shown in Fig. 3.7, at operating point (b), the circulating energy is much larger than at operating point (a). With a lower power factor, more energy should be sent back to the source during each switching cycle and more energy needs to be processed by the semiconductors and resonant tank, and therefore raise the conduction loss. On the other hand, with higher power factor, devices can turn off at a lower current, meaning a reduction of turn-off loss.

In summary, the power factor is an important property to determine the efficiency of the resonant converter. It is desirable for resonant converters to operate at high power factor mode. Thus, low conduction loss and low switching loss can be achieved. An optimal design based on the power factor concept will be investigated in the following chapter.

The described analysis and procedure can be easily extended to any other resonant converter.

Chapter 4

Resonant Converter Design and Optimization for Pulsed Power Supplies

4.1 LCC and PRC Resonant Converter

4.1.1 Introduction

In previous chapters, the trends and technical challenges for pulsed power systems were discussed. High power density, high efficiency and high frequency are the major goals for this application. A topology capable of higher switching frequency with higher efficiency is the key to achieve these goals. Resonant converters have many advantages over PWM converters. They have lower switching losses at higher switching frequencies, easier EMI filtering, circuit parasitics absorption and higher efficiency. For reasons such as these they have sparked an increasing interest over the past decade.

SRC, PRC and LCC resonant converters are the most popular topologies. There are several main disadvantages of the SRC: (i) The switching frequency varies directly with the load. This leads to poor cross-regulation in multi-output power supplies such as capacitor charging power systems. (ii) The SRC cannot absorb the transformer parasitic

capacitance, which has an adverse effect on the performance of the converter. (iii) The SRC can not operate at zero load. However, LCC and PRC resonant converters can fully absorb the high voltage transformer nonidealities and have full power control range with a small variation in frequency. Therefore, these two converters could be considered an optimum topology for pulsed power supply. In this chapter, LCC and PRC resonant converters will be evaluated for a capacitor-charging power supply.

4.1.2 DC Analysis of LCC and PRC Converters

The DC characteristic is the most important information for the converter design. With the DC characteristic, the parameters can be chosen; the design trade-offs can be made. For LCC and PRC resonant converters, the DC characteristic will define the relationship between voltage gain and switching frequency for different load condition.

Traditionally, fundamental element simplification method was used to analyze the DC characteristic of a resonant converter. The fundamental element simplification method (FEM) assumes only the fundamental component of switching frequency is transferring energy. With this assumption, the nonlinear parts of the converter, like switches and diode bridges, could be replaced with linear components. The simplified converter will be a linear network to analyze. So, with this method, the DC characteristic could be derived very easily. And the result will be a close-form equation, which is easy to use. Most of the literature on resonant converters provides the DC characteristic equations with fundamental element simplification method. However, these equations are only suitable for the LCC resonant converter with inductive output

filter. If a capacitive output filter is adopted, things are changed significantly. In this case, the diode rectifier only conducts part of the time during the cycle. Thus, the rectifier current and voltage are far from the regular square waveform or sinusoidal waveform. It is not adequate to use the well-known equivalent AC load resistor to model the resonant converter and derive the DC characteristic equation.

The detailed analysis of the LCC or PRC converter is complex because the capacitive output filter stage is decoupled from the resonant stage for a significant period within the switching cycle. As a result, the number of resonant elements changes during the switching cycle and thus the converter operates multi-resonantly. Ivensky proposed another analytical methodology for analysis of LCC and PRC resonant converter with capacitive filter [C-2]. In this model, the rectifier, output capacitor and load are replaced by an equivalent circuit which includes a capacitor and resistor connected in parallel. With this model, fundamental approximation method can be still used, but the derivation is much more complicated than the conventional model with simple equivalent AC resistor.

With the help of the AC model for LCC and PRC converters with a capacitive filter, DC characteristic equations can be derived as follows.

$$\theta = 2 \cdot a\tan(\sqrt{\frac{\pi}{2} \cdot \frac{1}{\omega_n \cdot Q_L \cdot (1 + C_n)}})$$

$$K_v = 1 + 0.27 \cdot \sin(\theta)$$

$$\beta = \frac{\pi}{180} \cdot (-25 \cdot \sin(\theta))$$

$$K_e = \frac{2 \cdot \tan(|\beta|)}{\omega_n \cdot Q_L \cdot K_v^2 \cdot (1 + C_n)} \cdot$$

$$\frac{V_o}{V_{in}} = \frac{\frac{\pi}{4 \cdot K_v}}{\sqrt{\left[1 + C_n + K_e \cdot C_n - \omega_n^2 \cdot (1 + K_e) \cdot (1 + C_n)\right]^2 + \left\{\frac{2 \cdot \left[\omega_n^2 \cdot (1 + C_n) - C_n\right]}{\omega_n \cdot Q_L \cdot K_v^2 \cdot (1 + C_n)}\right\}^2}}$$

$R_{eq} = R_o \cdot \frac{K_v}{2n^2}$ (Equivalent load resistor)

$C_{eq} = \tan(|\beta|) \cdot \frac{2n^2}{R_o \cdot \omega_n \cdot \omega_o \cdot K_v^2}$ (Equivalent load capacitor)

$Q_L = \frac{R_o}{Z_o \cdot n^2}$ (Load quality factor)

$Z_o = \sqrt{\frac{L_r}{\frac{C_r \cdot C_p}{C_r + C_p}}}$ (Characteristic impedance)

$C_n = \frac{C_p}{C_r}$ (Ratio of two resonant capacitors)

For this method, there are some limitations. Because this method is a simplified method, an error will be generated with different operating points. To evaluate this

error, a more accurate DC characteristic is needed. Here simulation is used to derive the accurate DC gain characteristic. A time-domain switch circuit model is built in simulation software such as SABER. By changing the switching frequency and load condition, an output voltage can be obtained for each point. Sweeping load and switching frequency, an accurate DC characteristic is achieved. The results of these two methods are shown in following figures, and the error is also shown.

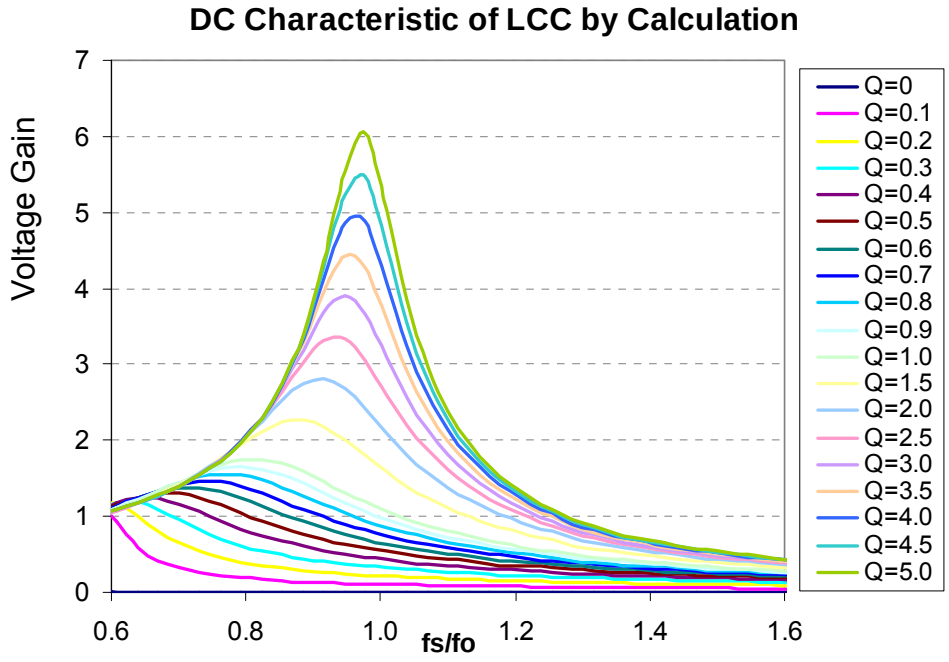

Fig. 4.1. DC characteristic of LCC from simplified model

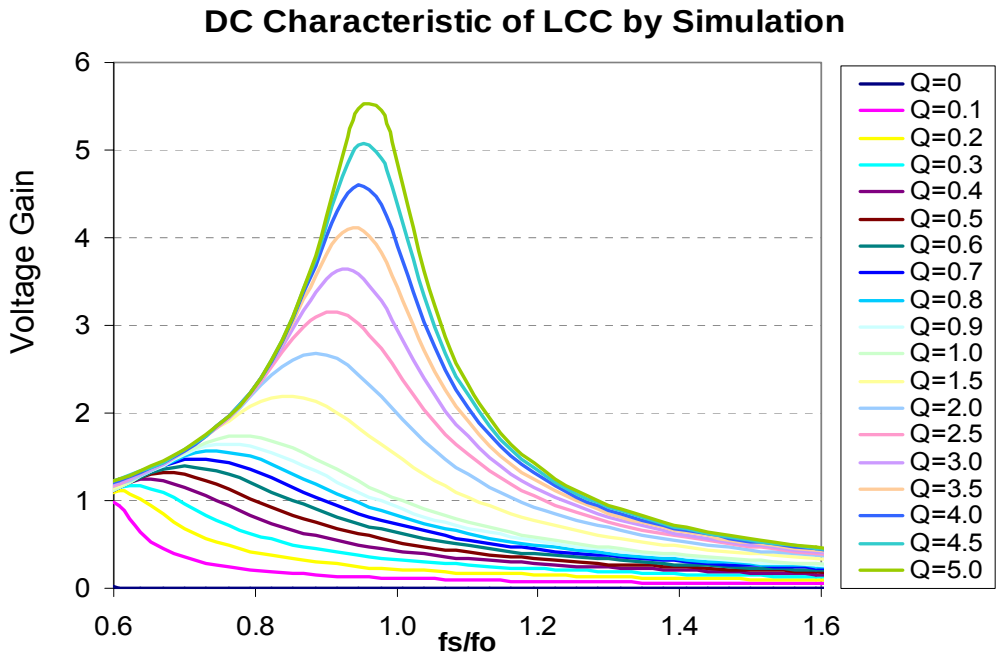

Fig. 4.2 DC characteristic of LCC from simulation method

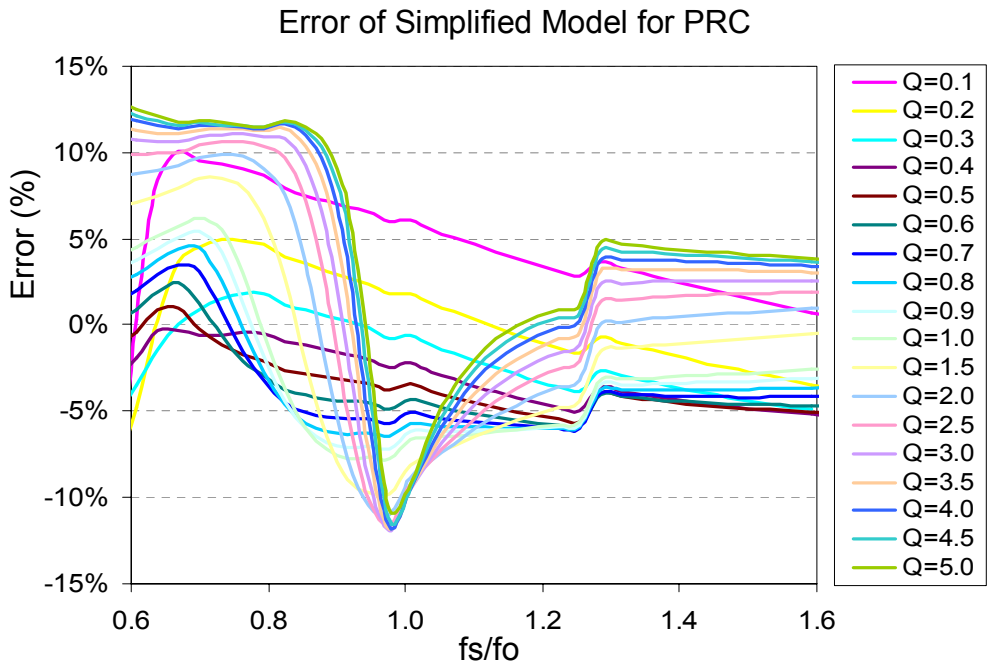

Fig. 4.3. Error of simplified circuit model for LCC

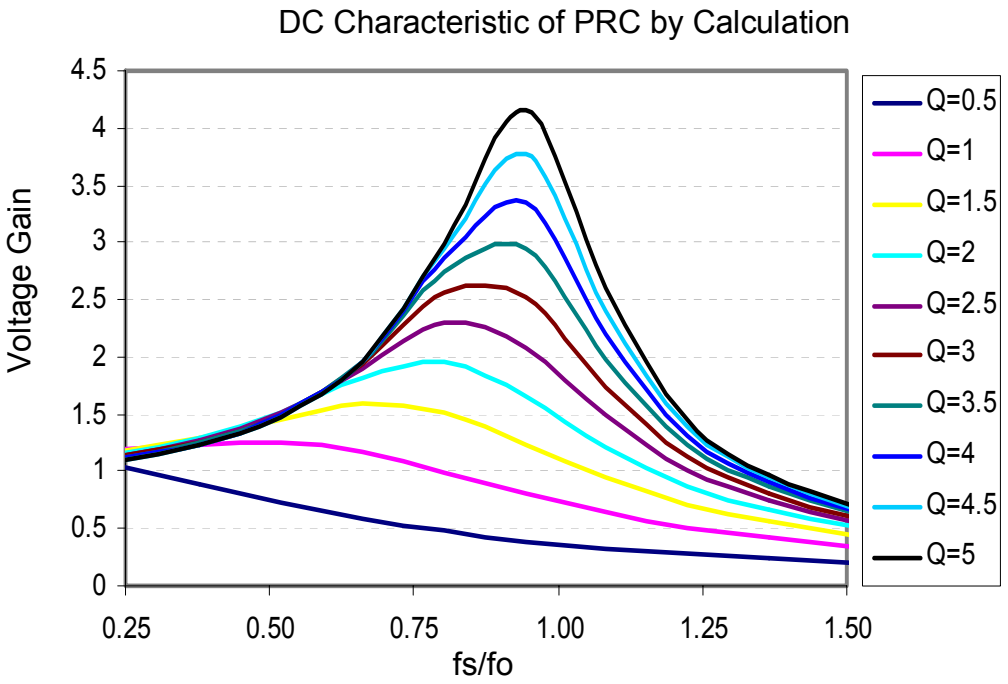

Fig. 4.4. DC characteristic of PRC from simplified model

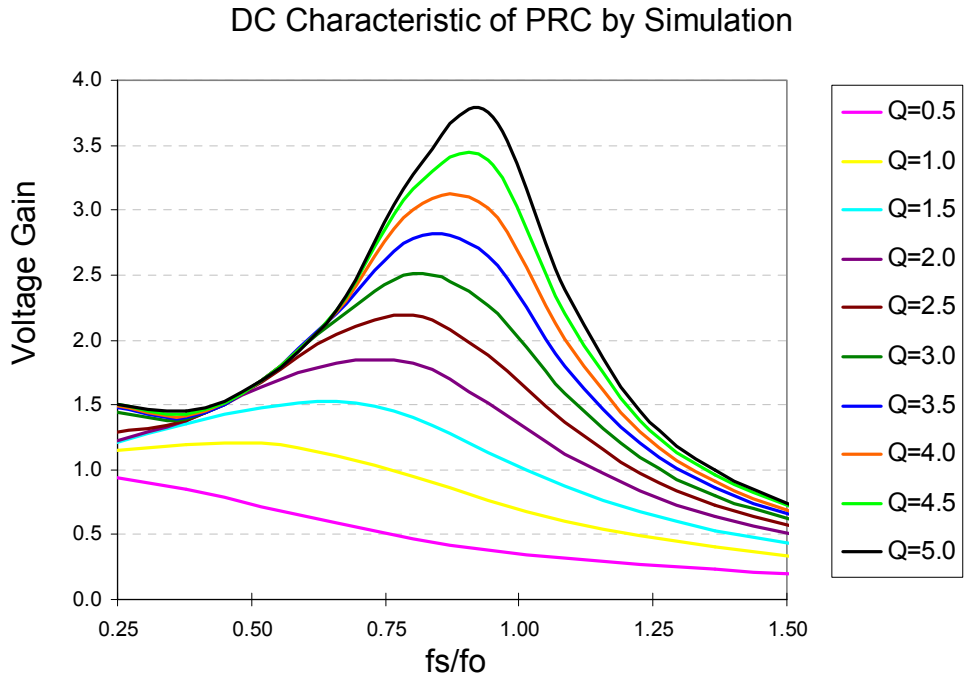

Fig. 4.5. DC characteristic of PRC from simulation method

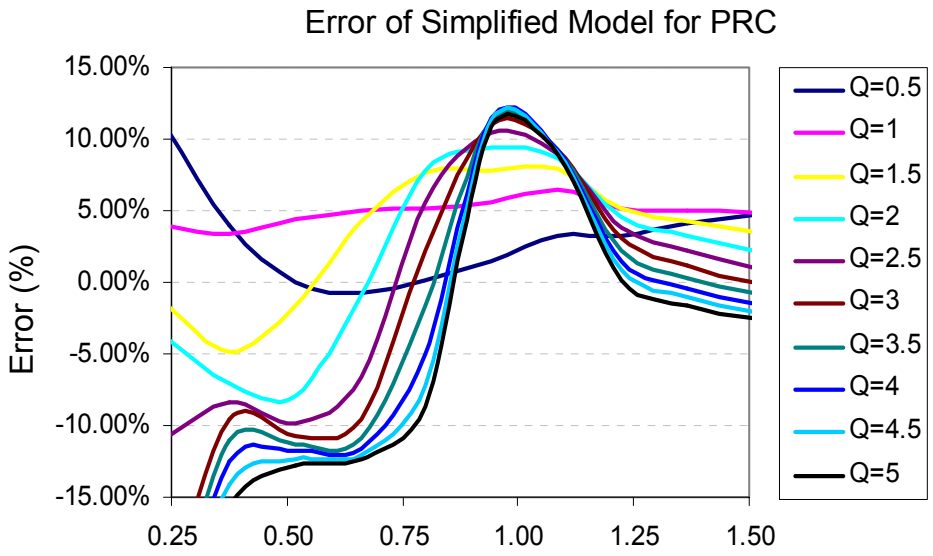

Fig. 4.6. Error of simplified circuit model for PRC

For the design of LLC resonant converter, the trade-offs are more affected by an operating point with maximum gain. With a simplified model, much error will be introduced. Simulation gives accurate results; the issue is that it is time-consuming. A better method is to combine these two methods. During primary design, use simplified model to get a trend. To optimize the design, simulation method is preferred to get a better design.

4.1.3 Operation of LCC and PRC converters

The DC characteristic of an LCC resonant converter could be divided into ZVS region and ZCS region as shown in Fig. 4.7. For this converter, there are two resonant frequencies. One is determined by the resonant components L_r and C_r. The other one is determined by L_r, C_r and C_p. As the load gets lighter, the resonant frequency will shift to higher frequency. The two resonant frequencies are:

$$f_o 1 = \frac{1}{2 \cdot \pi \cdot \sqrt{L_r \cdot C_r}}$$

$$f_o 2 = \frac{1}{2 \cdot \pi \cdot \sqrt{L_r \cdot \frac{C_r \cdot C_p}{C_r + C_p}}}$$

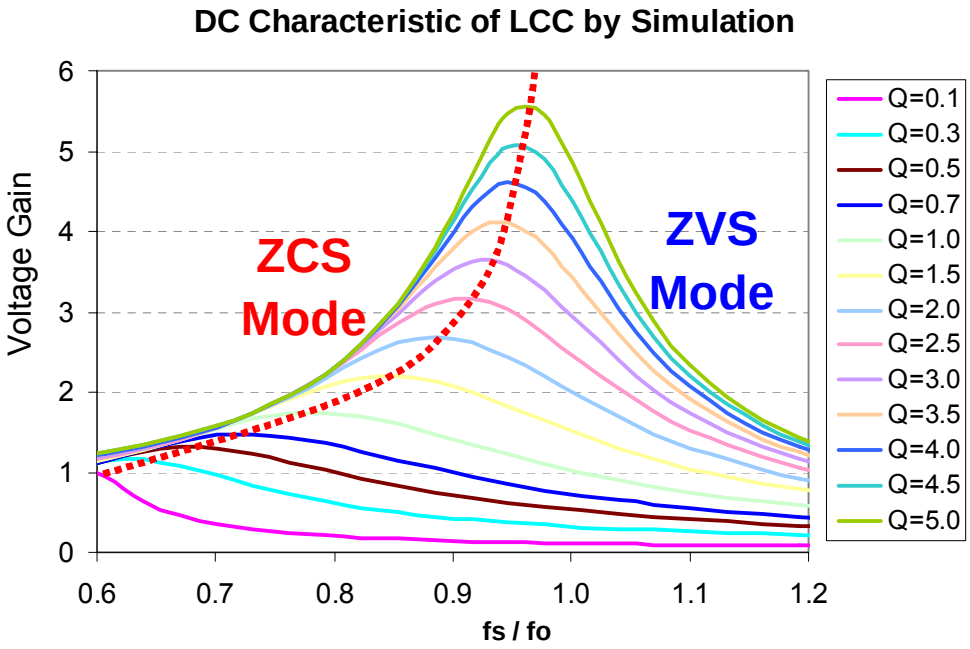

Fig. 4.7. Operation regions of LCC resonant converter

The LCC resonant converter exhibits intermediate characteristics between those of the SRC and PRC. When it operates with a heavy load, this converter has same characteristics of SRC. In the region near the $f_o 1$, SRC will be dominant. When the load gets lighter, characteristics of PRC will float to the top. With these interesting characteristics, when the load varies we could design the converter working along the

resonant ridge to achieve high efficiency. Advantages of both SRC and PRC can be utilized properly.

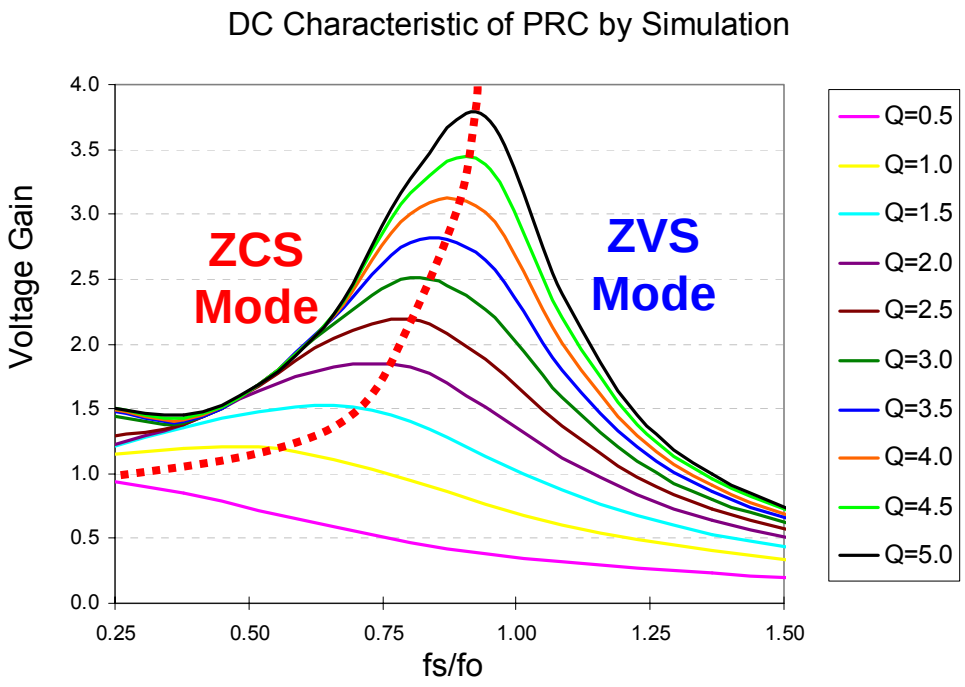

Fig. 4.8. Operation regions of PRC resonant converter

Similarly, the DC characteristic of PRC could be divided into ZVS region and ZCS region as shown in Fig. 4.8. For this converter, the corner frequency (undamped natural frequency) is determined by the resonant components L_r and C_p. For the conventional PRC with inductive filter, the resonant frequency is almost fixed at the corner frequency and does not change with the variation of loads. However, for the PRC with capacitive filter, as loads get lighter, the resonant frequency will shift to a higher frequency. As a result, the PRC for this application exhibits similar characteristics as an LCC converter. The analysis of LCC converters can be extended to that of PRC.

More importantly, when C_n (ratio of two resonant capacitors) of LCC turns to zero (the series capacitor becomes infinite or shorted), the LCC converter will become PRC. As a result, in this work, PRC is considered as a particular case of LCC when C_n is equal to zero.

4.2 Constant Power Factor Control Scheme for Resonant Converter

In the previous Chapter, it is pointed out that a hybrid charging scheme was chosen by existing literature for capacitor-charging power supplies. That is, a hybrid of constant current charging in the first stage of the charging period and constant power in the second stage of the charging period. For this control method, the normalized output current and the normalized output power are the most important parameters used to design the resonant tank. The surface plots of these two parameters against the Q and f_n have been shown in Fig. 4.9. The constant current charging trajectory can be depicted as the border line shown in Fig. 4.9 (a). It is noted that resonant converters could achieve constant output current when operating at this line. Similarly, the constant power charging trajectory can be illustrated in Fig. 4.9 (b). Resonant converters can achieve constant output power when operating at this line. On the other hand, these charging trajectories can be also mapped to voltage gain surface, which is shown in Fig. 4.10.

Based on this charging mode, careful selection of resonant tank parameters will lead to a good design to achieve high power density.

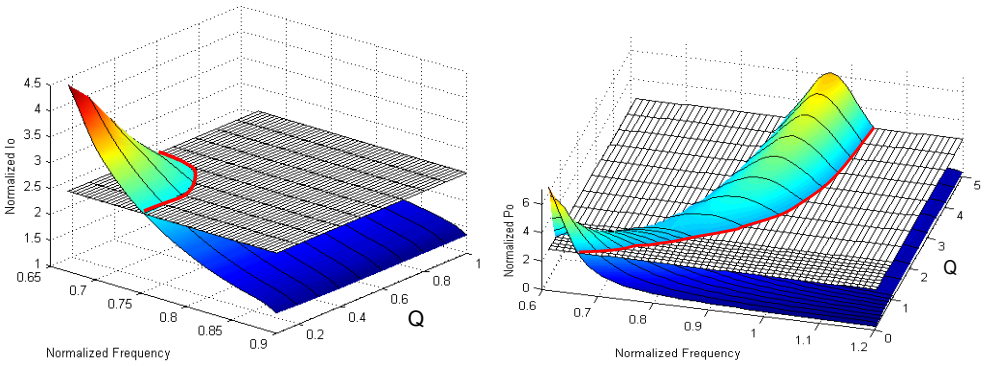

(a) Constant current trajectory on the normalized output current surface versus fs/fo and Q

(b) Constant power trajectory on the normalized output power surface versus fs/fo and Q

Fig. 4.9. Surface plot of I_{o_N} and P_{o_N}

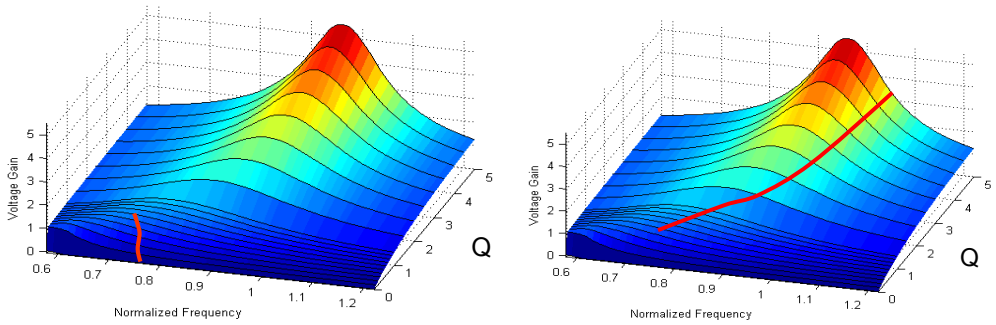

(a) Constant current trajectory on the normalized voltage gain surface versus fs/fo and Q

(b) Constant power trajectory on the normalized voltage gain surface versus fs/fo and Q

Fig. 4.10. Different charging trajectories on the surface of normalized voltage gain

The constant current charging trajectory is a line segment of Fig. 4.9 (a) or Fig. 4.10 (a). The constant power charging trajectory is a line segment of Fig. 4.9 (b) or Fig. 4.10 (b). Combining two charging trajectories, the complete charging profile is shown in Fig. 4.11 (a). In addition, the power factor of this design is shown in Fig. 4.11 (b).

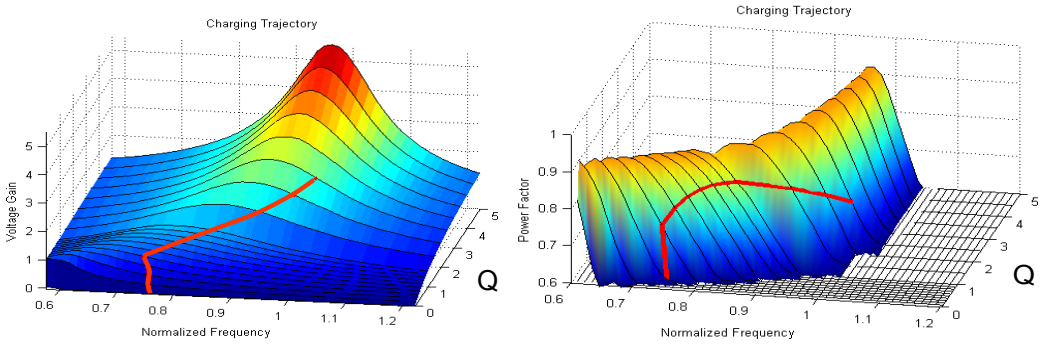

(a) The capacitor charging trajectory on the normalized voltage gain surface versus fs/fo and Q

(b) The capacitor charging trajectory on the power factor surface versus fs/fo and Q

Fig. 4.11. Charging trajectory of LCC resonant converter

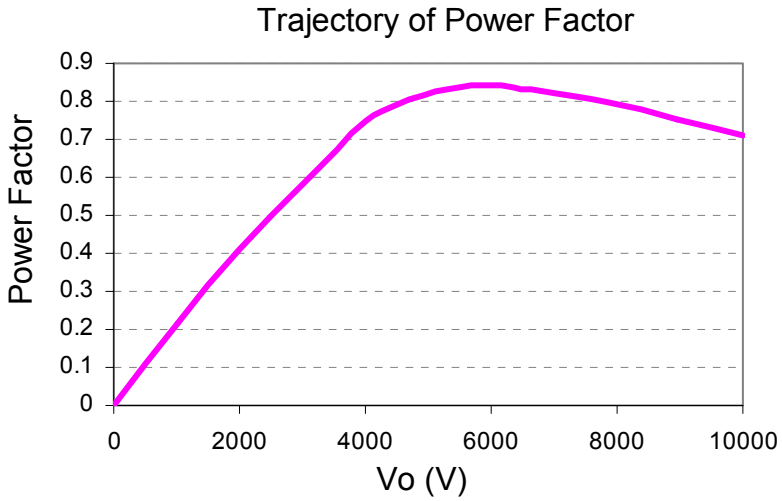

Fig. 4.12. Power factor versus output voltage for LCC converters

From Fig. 4.12, it can be observed that the power factor trajectory during the charging processing is variable with the output voltage. For this trajectory, there is only a short line segment whose value is above 0.8. Namely, the power factor is below 0.8 and the converter circulates more than 20% of the energy during most of the charging time. Though ZVS can help to reduce the switching loss effectively, the conduction loss of MOSFET is still high.

From Fig. 4.12 and Fig. 4.13, it can be seen that the lowest loss is achieved with the maximum power factor. In order to decrease the loss and increase the efficiency, it is desirable to improve the power factor of resonant converters. However, with the conventional constant current and constant power control methods, it is very difficult to achieve this.

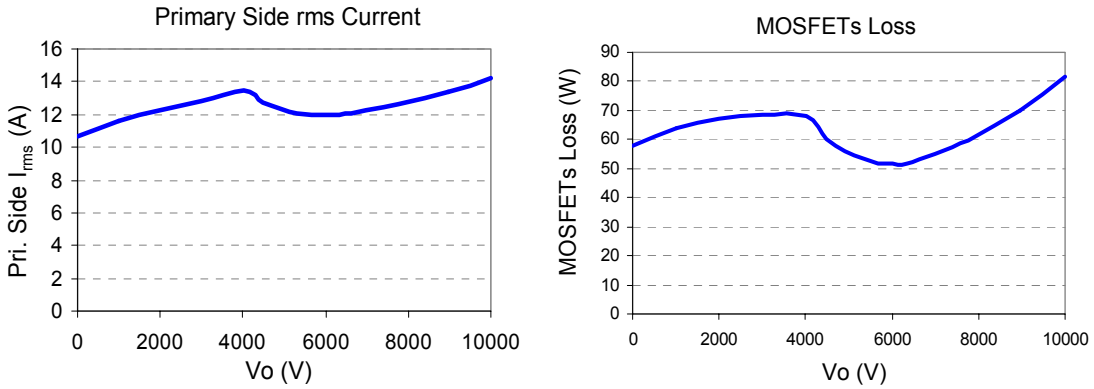

(a) The primary side rms current of LCC (b) The MOSFETs total loss

Fig. 4.13. Primary side rms current and MOSFETs loss

In this work, a new methodology is proposed to further improve the efficiency and performance of the resonant converter.

A promising method to decrease the circulating energy is to keep the power factor at a constant value as high as possible during the charging time. Based on this concept, a novel constant power factor control method is proposed. For this control scheme, the switching frequency is variable and regulated to maintain the constant power factor of the resonant converter during the operation.

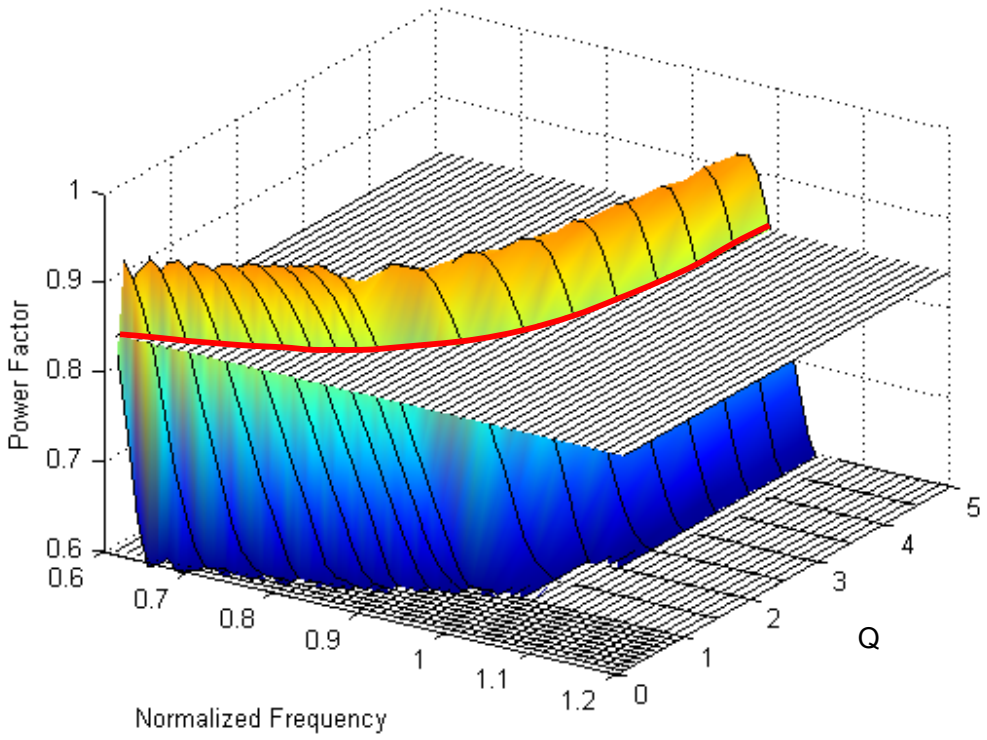

Fig. 4.14. An operation trajectory for constant power factor control method

With the expression of $PF = \frac{P_{o\_N}}{I_N}$, the normalized power factor of resonant converters can be calculated. Therefore, with the variation of loads, the switching frequency can be regulated to obtain the anticipated value of power factor. The operation trajectory is the border line of a horizontal plane and the power factor surface, as shown in Fig. 4.14. When resonant converters operate along this line, the power factor can be achieved as a constant value. It can be found that the higher power factor leads to lower circulating energy and higher system efficiency. However, excessively operating close to the resonant frequency will result in little turn-off current which can not guarantee ZVS operation. Furthermore, due to the effect of noise, the converter will run into the ZCS operation region. For power MOSFETs, zero voltage switching is

preferred. ZCS operation will degrade the performance of the converter. As a result, $PF = 0.84$ is considered a suitable value to obtain high power factor and guarantee ZVS operation.

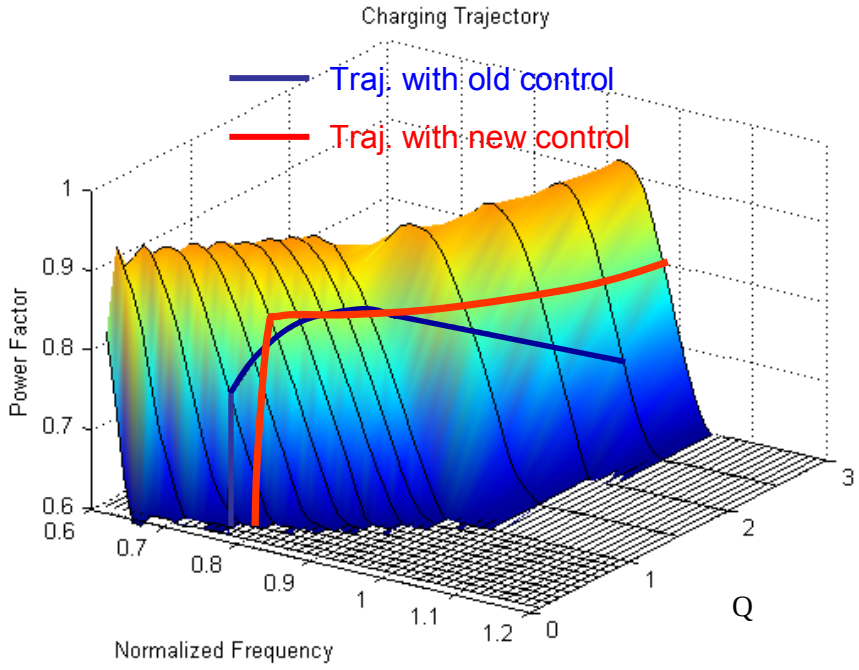

Fig. 4.15. Charging trajectories comparison during the whole period

The charging trajectory of constant power control method is illustrated in Fig. 4.15. The power factor of the resonant converter remains a constant value—0.84. Comparing this with the constant power control, it can be derived that the converter will reduce a lot of circulating energy and therefore higher efficiency can be achieved. The optimal constant power factor scheme is an attractive control method. However, it cannot be accomplished during the entire charging period. At the beginning of the charging process, the voltage of the load capacitor is very low. This leads to the very low Q. To maintain the high power factor at a low Q, the converter needs to operate at very high

power levels which will exceed the input capability. As a result, a combined charge method is adopted for this application. The principle is to start the charge process by applying a constant-current charge mode. When the load capacitor is charged, the output voltage will increase. The power factor of the converter will also increase. Once the power factor reaches the predetermined value, the converter will change to constant power factor charge mode.

For the sake of simplicity, the hybrid constant current and constant power control is written as CCCP, while the new constant current and constant power factor control is written as CCCPF.

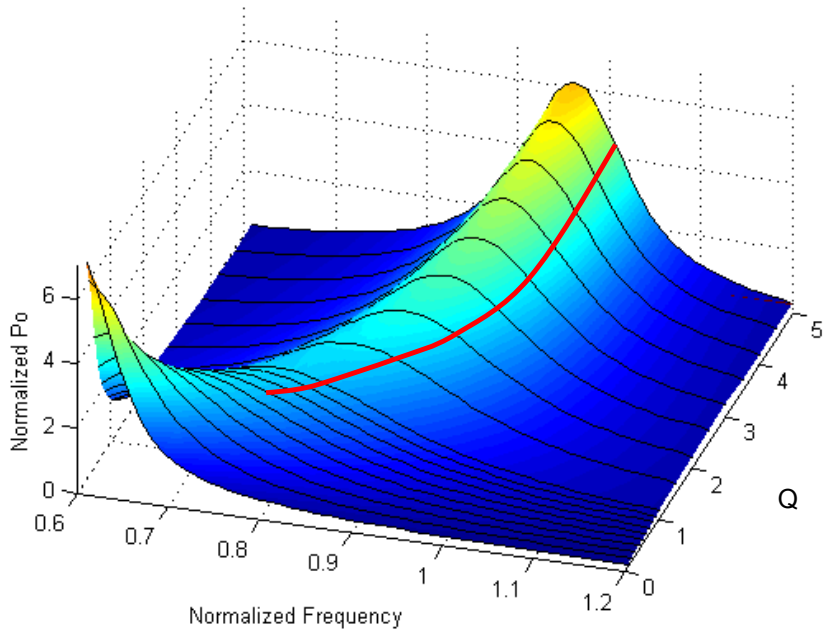

Fig. 4.16. CCCPF charging trajectory shown on the 3D surface of normalized output power

The optimal design based on the CCCPF will be investigated in the following sections.

4.3 Resonant Converter Optimal Designs Based on Power Factor Control Scheme

4.3.1 Design Introduction

In previous section, the charging scheme was chosen, constant current charging in the first stage and constant power factor charging in the second stage. Based on this charging mode, we will design the pulse power supply with the highest power density.

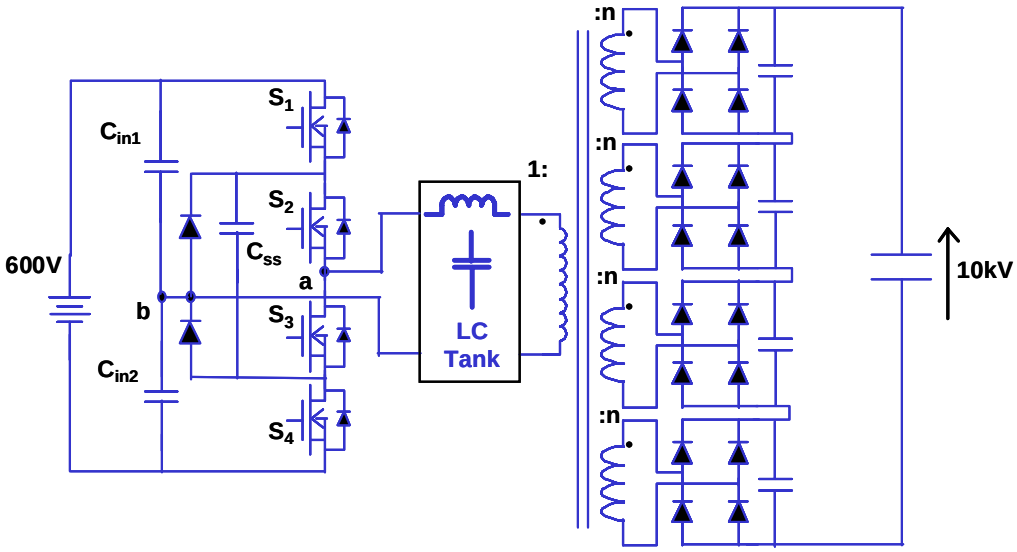

Fig. 4.17. The topology chosen for pulsed power supplies

The circuit structure is shown in Fig. 4.17. The characteristics of this topology were discussed in the previous chapter. The objective is to design the resonant tank, i.e., the resonant inductor, resonant capacitor, and the transformer, to achieve high efficiency and high power density.

High frequency is expected to minimize the size of the passive components. However, it is limited by the switching loss of the secondary diodes. Operating at very

high switching frequency, High-voltage diodes' reverse recovery problem becomes very severe. High-voltage diodes' reverse recovery characteristics have been tested and the result is shown in Fig. 4.18. It can be seen that 200 kHz switching frequency is a good choice for safe operation. Therefore, it is assumed that the highest switching frequency is 200 kHz. This assumption is valid throughout the design procedure. With this assumption, designs are compared to find out the guideline for the low power loss and minimum converter volume.

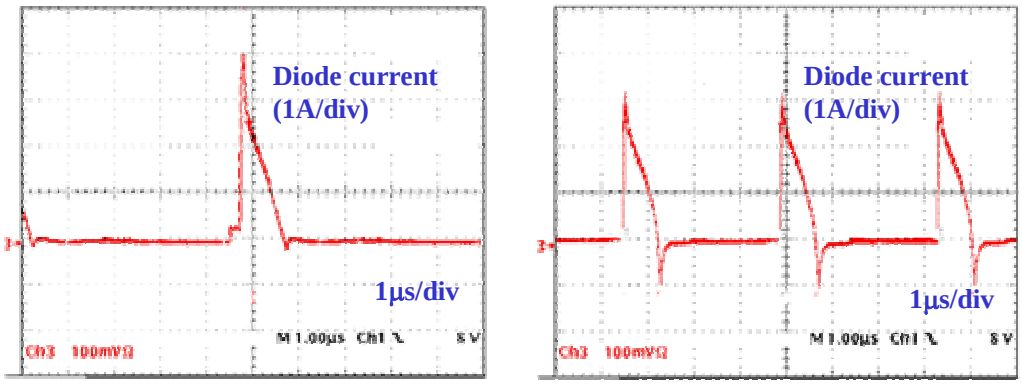

(a) Operating at 200 kHz (b) Operating at 300 kHz

Fig. 4.18. Reverse recovery test waveform for 1N6863 (2kV, 30n) with different operation frequencies

From the charging mode proposed in the previous section, the following specifications can be given.

(a) The initial constant charging current is 0.75 A.

(b) The highest switching frequency is set as 200 kHz.

(c) The total charging time is 7.73 S (< 8 S).

(d) Because three-level structure is applied, the input voltage of the resonant tank is half of the input DC bus; that is 300 V.

(e) $C_n = C_p / C_r = 0.5$ is adopted.

For the design with CCCPF control, the constant power factor is set as 0.84. From Fig. 4.14, $Q = 2.5$ and $f_n = 0.97$, are chosen at the operating point of 10 kV and 200 kHz. $f_o = 206.2$ kHz can be calculated. For this operation point, $M = 3.37$, due to $M = V_o / (V_{in} \cdot n)$ transformer turns ratio will be 10. From Fig. 4.16, it can be observed that $P_{o\_N} = 3.8$ for this operating point. For CCCPF control, the output power is not constant but variable. The output power is set as 3.7 kW at this operating point. From $P_{o\_N} = P_o / (V_{in}^2 / Z_o)$, $Z_o = 92\Omega$. Therefore, the value of resonant tank can be derived from $C_n = C_p / C_r = 0.5$, $f_o = \frac{1}{2\pi} \cdot \sqrt{\frac{1}{L_r \cdot \frac{C_r \cdot C_p}{C_r + C_p}}}$ and $Z_o = \sqrt{\frac{L_r}{\frac{C_r \cdot C_p}{C_r + C_p}}}$, then $L_r = 70.8$ μH, $C_r = 25.2$ nF and $C_p = 12.6$ nF, which is referred to primary side. The constant power factor charging trajectory of this design is a line segment of trajectory shown in Fig. 4.14. $V_o = 3.8$ kV is the critical point at which the charging mode turns from constant-current charge into constant power factor charge. At this point, $M = 1.29$ and $Q = 0.6$ can be calculated and $f_n = 0.77$ can be observed from Fig. 4.20. During the constant-current charge mode, $I_o = 0.71$ A and $I_{o\_N} = I_o \cdot n / (V_{in} / Z_o) = 2.2$ are obtained. The constant-current charging trajectory of this design is shown in Fig. 4.19.

Combining the two charging trajectories, the complete charging profile can be illustrated on voltage gain surface, which is shown in Fig. 4.20.

In Fig. 4.20, the charging trajectory of CCCP is also depicted. It can be observed that the charging trajectory of CCCPF is closer to the resonant frequency than that of CCCP. It results in lower circulating energy and lower turn-off current, which reduce the MOSFET loss effectively. Higher efficiency can be achieved.

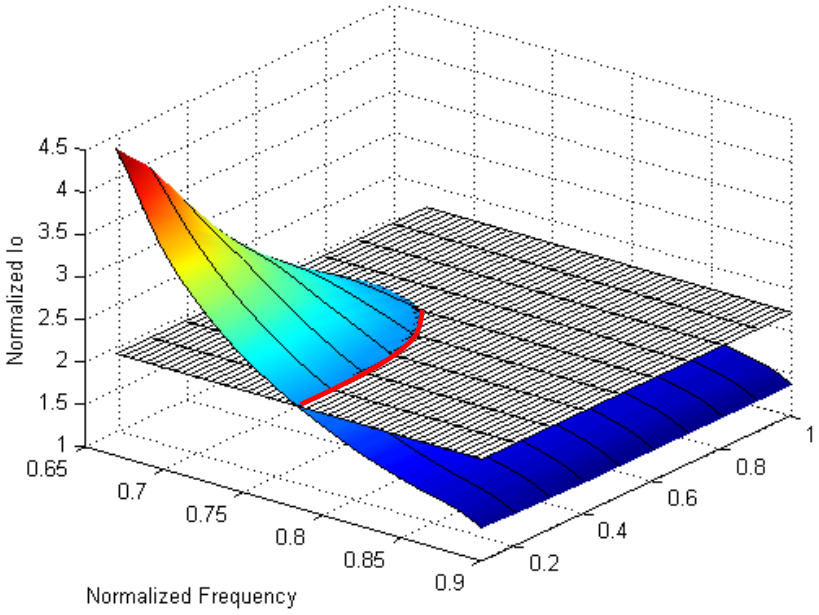

Fig. 4.19. Constant current charging trajectory for CCCPF control

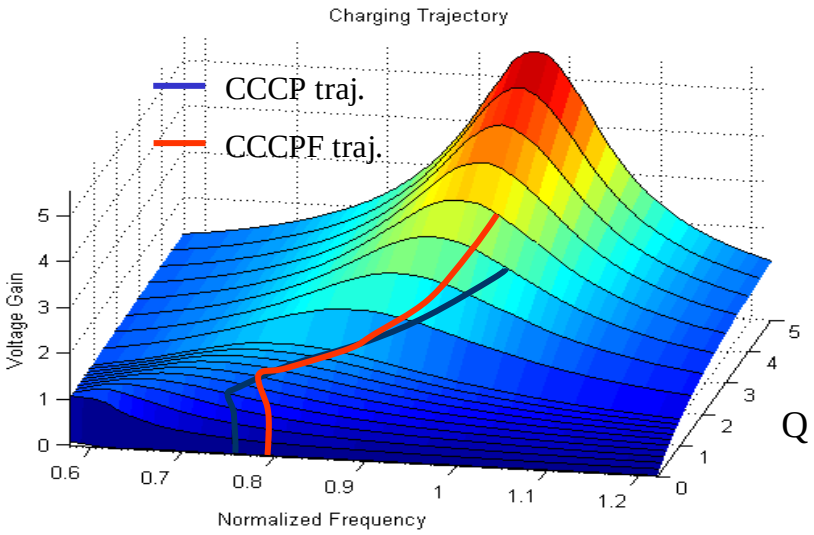

Fig. 4.20. Charging trajectories of different control methods on the surface of voltage gain

The design result of CCCPF and CCCP are compared and shown in Table 4-1.

Table 4-1. Design result for different control schemes

Control Mode	CCCPF	CCCP
C_n	0.5	0.5
M at 10 kV	3.37	2.6
Q at 10 kV	3.0	2.5
L_r (Prim.-side)	70.8 μH	62.4 μH
C_p (Prim.-side)	12.6 nF	15.0 nF
C_r (Prim.-side)	25.2 nF	30.0 nF
Z_o	92 Ω	79.0 Ω
f_o	206.2 kHz	202 kHz
N_p:N_s	1:10	1:13
f_s Range	158~200 kHz	149~200 kHz

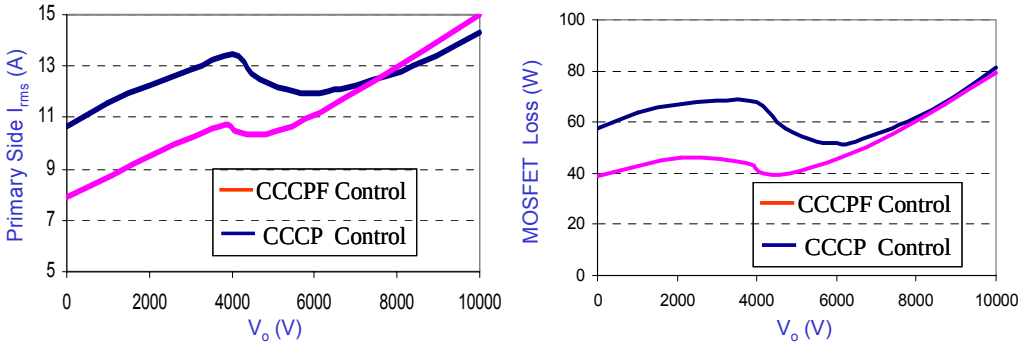

(a) Comparison of rms current for primary side with different control

(b) Comparison of MOSFET loss with different control

Fig. 4.21 RMS current and MOSFET loss comparison for different control methods

The CCCPF control scheme can fully utilize the capability of the resonant tank to transfer the power to the output. More importantly, during the power delivery, the high efficiency could be obtained. This can be demonstrated from the loss comparison shown in Fig. 4.21.

4.3.2 Trade-off Designs for the Fixed Value of C_n

The previous section shows that the novel constant power factor control can reduce the circulating energy of resonant converters and improve their performance. In this section, based on CCCPF control, optimum design aiming to increase the power density will be provided.

For $C_n = 0.5$ and $PF = 0.84$, the several designs will be obtained if different values of f_n and Q are chosen at the operating point of 10 kV and 200 kHz. Following the aforementioned design procedure, several designs can be made. These different design

parameters are shown in Table 4-2 for comparison. The charging trajectories of these designs are illustrated in Fig. 4.22 and Fig. 4.23.

Table 4-2. Comparison for different designs with new CCCPF control

	Design D	Design E	Design F
C_n	0.5	0.5	0.5
M at 10 kV	2.1	3.37	4.7
Q at 10 kV	1.5	3.0	4.5
L_r (Prim.-side)	60.1 μH	70.8 μH	87.9 μH
C_p (Prim.-side)	25.8 nF	12.6 nF	21 nF
C_r (Prim.-side)	12.9 nF	25.2 nF	10.5 nF
Z_o	83.5 Ω	92 Ω	112 Ω
f_o	221.0 kHz	206.2 kHz	202.6 kHz
N_p:N_s	1:16	1:10	1:7
f_s Range	150~200 kHz	158~200 kHz	156~200 kHz

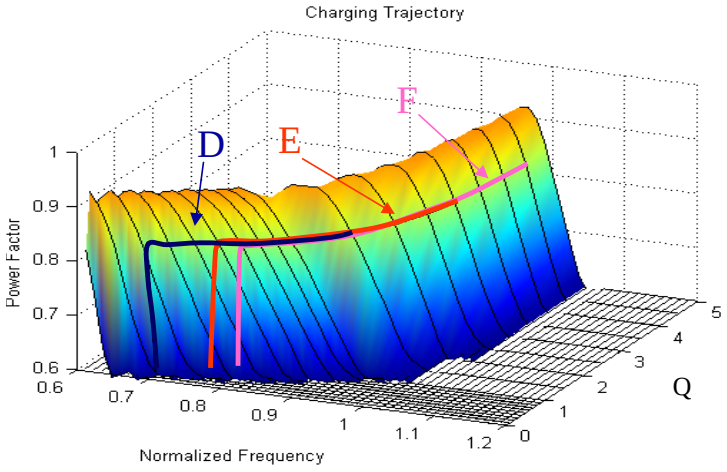

Fig. 4.22. Charging trajectories for different designs on power factor surface

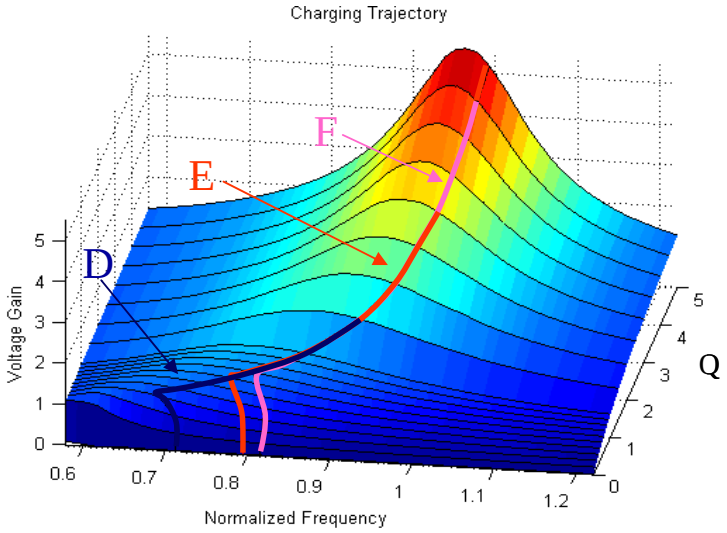

Fig. 4.23. Charging trajectories for different designs on voltage gain surface

The rms current of primary side and MOSFET loss for different designs (labeled D, E and F) are shown in Fig. 4.24. It can be observed that: for the part with constant power factor control, the difference of MOSFET loss for different designs is minor. However, for the part of constant current control, the loss is totally different. Because the power factor can not be effectively controlled during this period, the higher the initial charging current (design D), the more circulating energy will be generated. In order to reduce the loss, low charging current is preferred during the constant-current charge mode. But excessive low initial charging current (design F) will require high power capability of the converter. Therefore, the current and voltage stress will increase. Design E is a good trade-off to obtain low loss and low current stress.

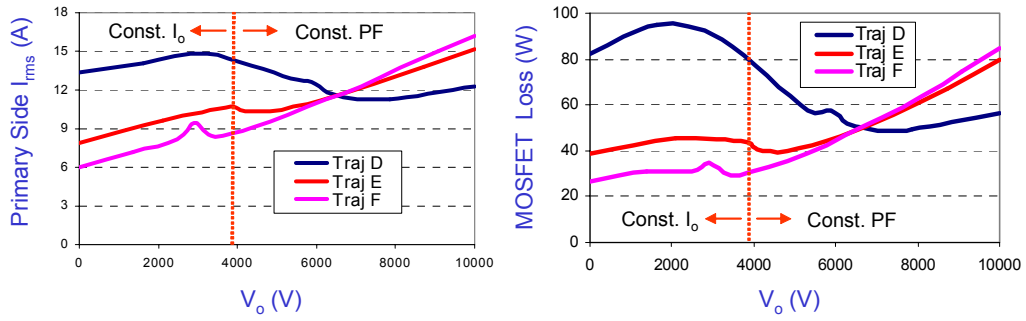

(a) Comparison of rms current for primary side with different designs

(b) Comparison of MOSFET loss with different designs

Fig. 4.24. RMS current and MOSFET loss comparison for different designs

As discussed previously, a good design is not only reliant on the high efficiency but also on the passive components' size. In Fig. 4.25, comparison for different designs is given. In Fig. 4.25 (a), the instantaneous device losses of the three designs are illustrated. It can be seen that the device loss is high for design D in the low-output-voltage region, while it is high for design F at high-output-voltage region, and design E is located between the two. Similarly, it is found that the volt-second of inductor and voltage stress of the series capacitor are high for design F in the high-output-voltage region. For design D, these happen in the low-output-voltage region. And for design E, the stresses are distributed more evenly. When the transformer volt-second is taken into account, the transformer size of design D should be larger than design E and design F. The transformer volt-second of design F is slightly less than that of design E. For series resonant capacitors, design D and design F both have much higher voltage stress than design E. Finally, design E is shown as an optimal design based on so many involved trade-offs mentioned above.

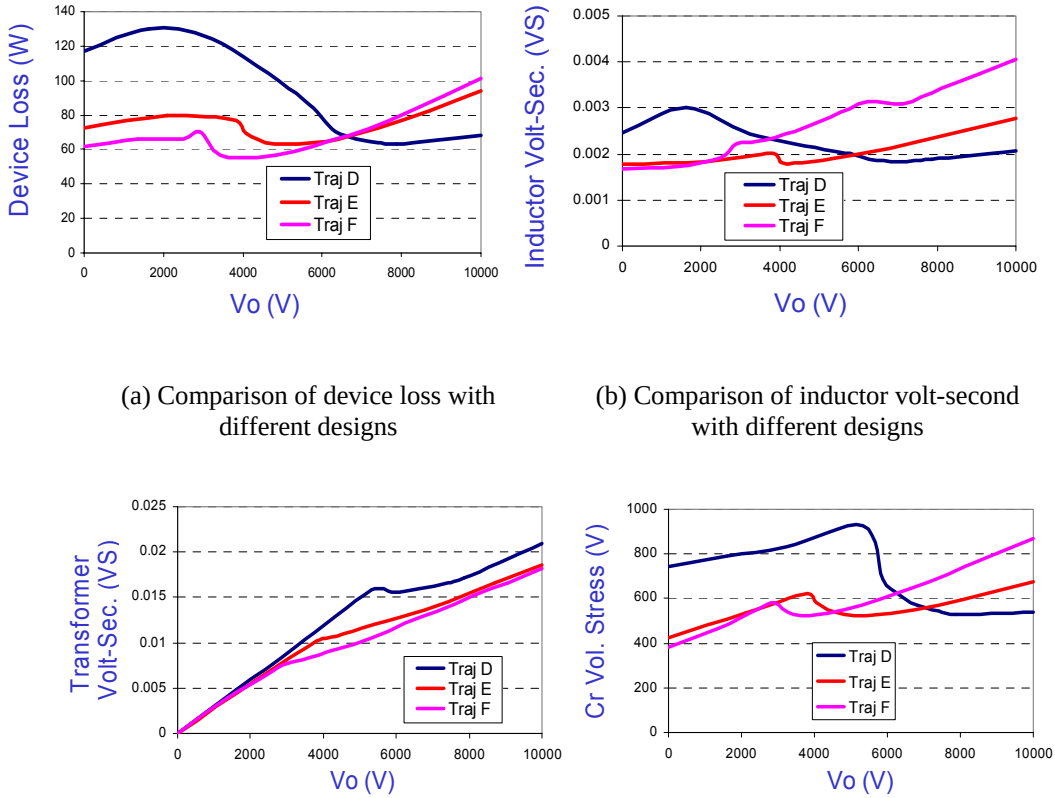

(a) Comparison of device loss with different designs

(b) Comparison of inductor volt-second with different designs

(c) Comparison of transformer volt-second with different designs

(d) Comparison of voltage stress on series capacitor with different designs

Fig. 4.25. Performance comparison of LCC resonant converter for different designs with new CCCPF control method

By applying the new CCCPF control method, the reactive power of resonant converters can be reduced and gain higher efficiency. But the characteristics of passive components will change also. An entire comparison between the two proposed control schemes including variation of passive components is necessary. The comparison result is shown in Fig. 4.26.

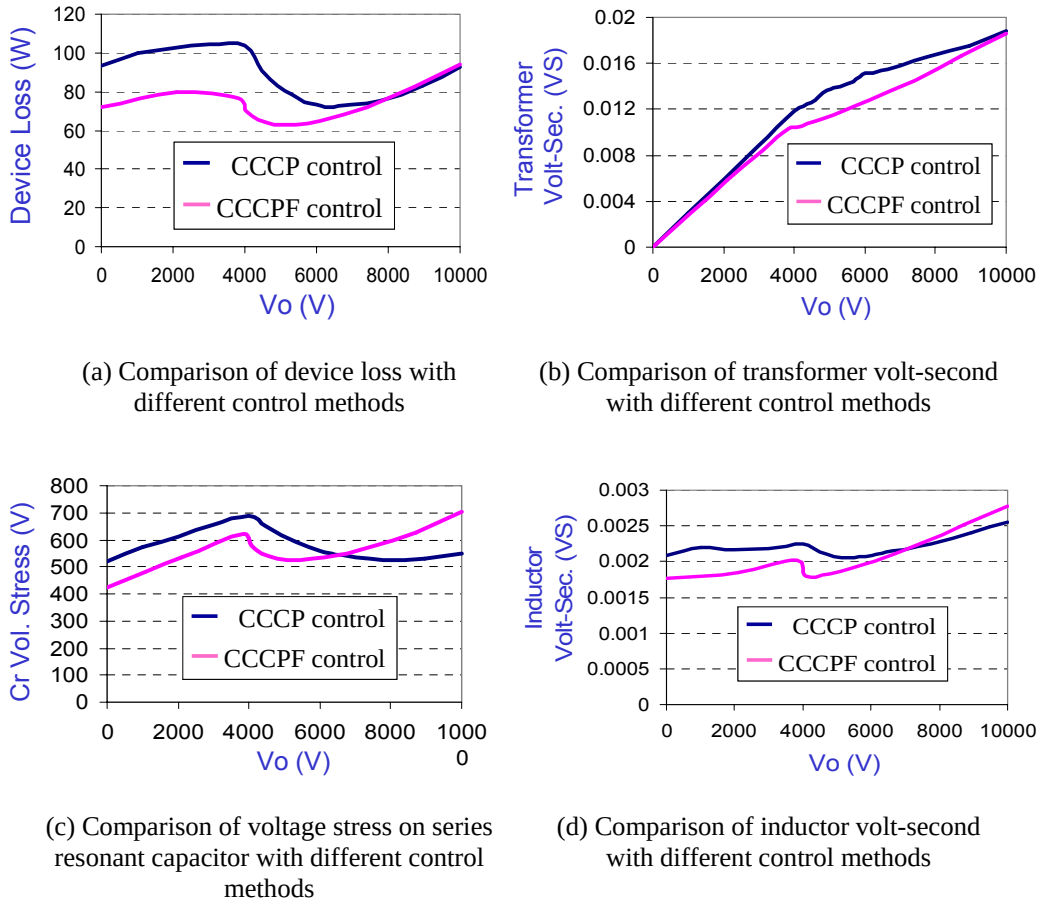

(a) Comparison of device loss with different control methods

(b) Comparison of transformer volt-second with different control methods

(c) Comparison of voltage stress on series resonant capacitor with different control methods

(d) Comparison of inductor volt-second with different control methods

Fig. 4.26. Design comparison for different control methods

It can be observed that there are pros and cons for the new CCCPF control. The benefits are: the device loss can be reduced and transformer volt-second turns slightly lower. The drawbacks are obvious: the inductor volt-second increases and voltage stress on the series resonant capacitor also increases. It seems that when C_n (ratio of resonant capacitances) is equal to 0.5, the new control method cannot improve the performance of the passive components. Therefore, the size of passive components can no be reduced; on the contrary, it will increase a little bit. This was not expected. Further investigation is still necessary.

4.3.3 The Optimal Design for Capacitor Chargers

C_n, ratio of resonant capacitances is another important parameter, which is worth considering seriously.

Table 4-3 Optimal designs comparison for different C_n

Control Mode	CCCPF	CCCPF
C_n	0.5	0.1
M at 10 kV	3.37	3
Q at 10 kV	3.0	3.5
L_r (Prim.-side)	70.8 μH	47 μH
C_p (Prim.-side)	12.6 nF	12.8 nF
C_r (Prim.-side)	25.2 nF	128 nF
Z_o	92 Ω	63.5 Ω
f_o	206.2 kHz	214.8 kHz
N_p:N_s	1:10	1:11
f_s Range	158~200 kHz	110~200 kHz

$C_n = 0.1$ is chosen for the next design. The constant power factor is set as 0.84. There are many designs if initial and end operating points are chosen differently. All these designs can be compared and the optimal design should be a good trade-off. At 10 kV, 200 kHz operating point, if Q is chosen as a low value (<1.5), then current and voltage stresses of the resonant converter will be high at the low-output-region. And if Q is chosen as a high value (>4.5), then current and voltage stresses of the resonant converter will be high at the high-output-region. Both of these two cases (low Q and

high Q) will lead to high electrical stress of the converter, which degrade the performance of the resonant converter. Consequently, the value of Q is recommended to be between 2 and 4 for the overall good performance of resonant converters.

Based on the above analysis, the optimal choice is the design whose current and voltage stresses are relatively low and evenly distributed during the entire charging period. The Q at the end of the charging trajectory is set as 3.5. This optimal design with $C_n = 0.1$ is shown in Table 4-3 and compared with the previous design for $C_n = 0.5$.

The charging trajectory of the design is shown in Fig. 4.27 and Fig. 4.28 respectively.

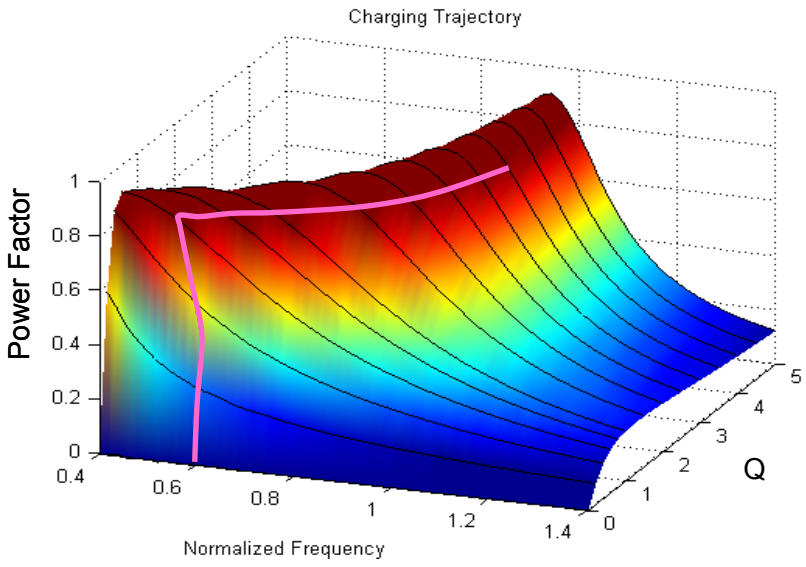

Fig. 4.27. Charging trajectory on power factor surface with $C_n = 0.1$

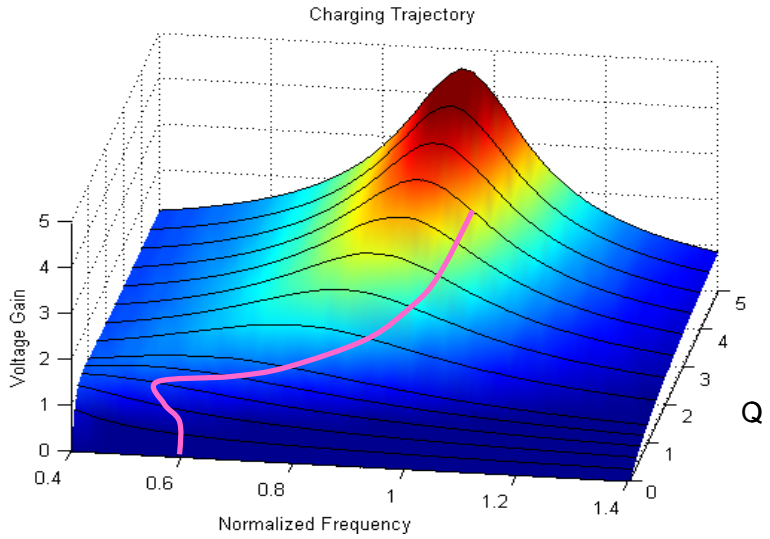

Fig. 4.28. Charging trajectory on voltage gain surface with $C_n = 0.1$

The performance of the resonant converter with different C_n is compared and shown in Fig. 4.29.

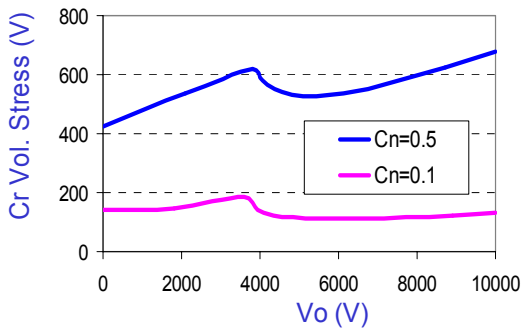

(a) Comparison of voltage stress on series resonant capacitor with different C_n

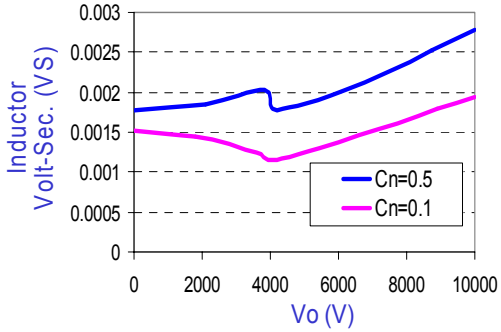

(b) Comparison of inductor volt-second with different C_n

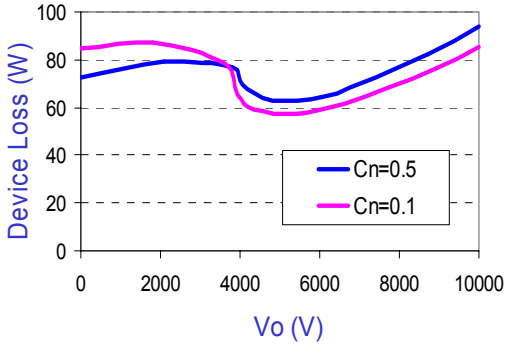

(c) Comparison of device loss with different C_n

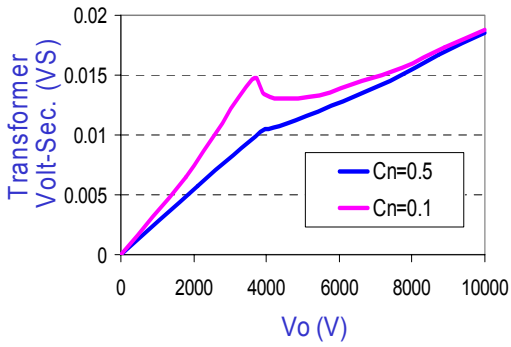

(d) Comparison of transformer volt-second with different C_n

Fig. 4.29. Design comparison for $C_n = 0.1$ and $C_n = 0.5$

It is obvious that the performance of the resonant converter is improved by a change the value of C_n. As seen from Fig. 4.29 (a), with the lower C_n, the voltage stress of the series resonant converter is reduced. From Fig. 4.29 (b), the inductor volt-second is lower when C_n becomes less. Meanwhile, the device loss and transformer volt-second don't change too much. The difference is minor. As a result, when C_n is reduced, the passive components size will be shrunk and the efficiency of the converter won't reduce.

It should be expected: if C_n is reduced even less, the power density of the resonant converter will be probably be improved.

The method is to push C_n into infinite smallness, namely turn it to zero. The LCC resonant converter will become PRC. For this application, the characteristic of PRC is

very similar to the LCC converter. Therefore, it is very convenient to follow the same design procedure of LCC.

Table 4-4. Optimal designs comparison for different C_n

Control Mode	CCCPF	CCCPF	CCCPF
C_n	0.5	0.1	0 (PRC)
M at 10 kV	3.37	3	3
Q at 10 kV	3.0	3.5	4
L_r (Prim.-side)	70.8 μH	47 μH	40.8 μH
C_p (Prim.-side)	12.6 nF	12.8 nF	13.3 nF
C_r (Prim.-side)	25.2 nF	128 nF	/
Z_o	92 Ω	63.5 Ω	55.4 Ω
f_o	206.2 kHz	214.8 kHz	215.7 kHz
N_p:N_s	1:10	1:11	1:11
f_s Range	158~200 kHz	110~200 kHz	80~200 kHz

For the PRC design with the CCCPF control, the constant power factor is set as 0.84. At 10 kV, 200 kHz operating point, if Q is chosen as a low value (<2), then current and voltage stresses of the resonant converter will be high at the low-output region. And if Q is chosen as a high value (>5), then current and voltage stresses of the resonant converter will be high at the high-output region. Both of these two cases (low Q and high Q) will result in high-current stress of the resonant inductor and the high volt-second of the transformer, which increase the volume of the magnetic components.

Consequently, the value of Q is recommended to be between 2 and 5 for the overall good performance of resonant converters.

These design parameters with PRC ($C_n = 0$) are shown in Table 4-4 and compared with the previous design for different C_n.

The charging trajectory of the design is shown in Fig. 4.30 and Fig. 4.31 respectively. It should be noted that with the new proposed constant power factor control, the performance of PRC is improved significantly. For the conventional design, when PRC operates at high Q or a light load, it suffers large circulating energy. If the voltage regulation varies within a wide range, the PRC will circulate more energy and result in very poor efficiency. Therefore, the PRC is seldom considered as a candidate for this application in the existing literature. However, in this work, the proposed constant power factor control scheme will enable the resonant converter to operate at high-power factor mode. This overcomes the adverse effect of load variation and wide voltage regulation. More importantly, if optimal design is achieved, the PRC will exhibit good performance and become a good candidate for this capacitor-charging application.

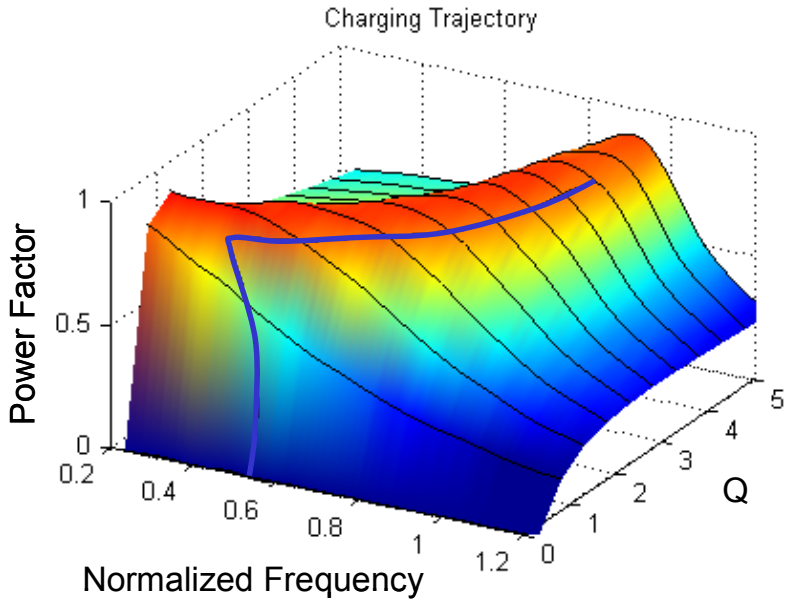

Fig. 4.30. Charging trajectory on power factor surface for PRC

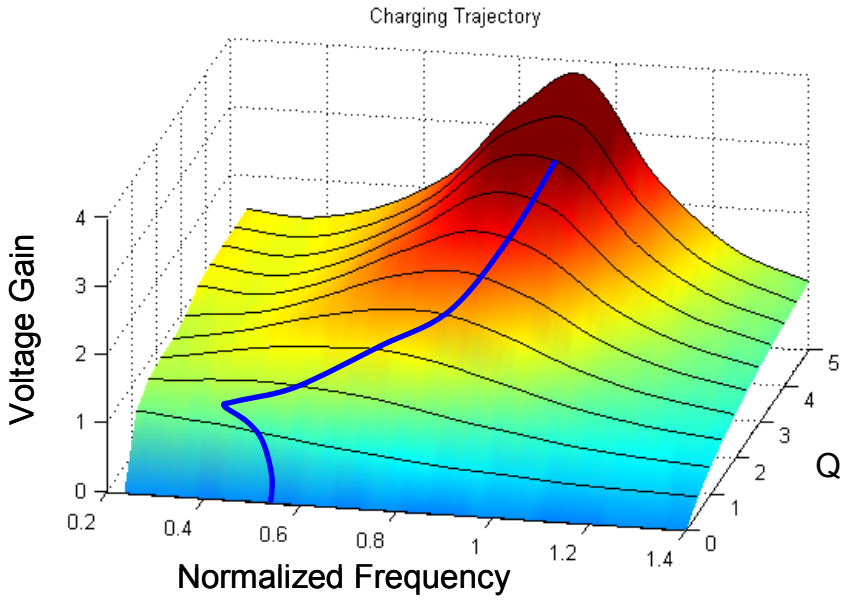

Fig. 4.31. Charging trajectory on voltage gain surface for PRC

The performance of the resonant converter for different C_n is shown in Fig. 4.32.

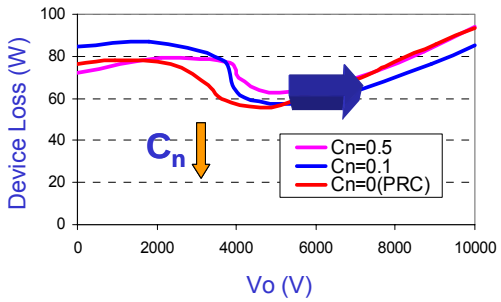

(a) Comparison of device loss with different C_n

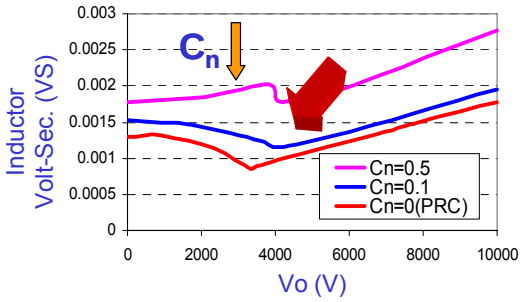

(b) Comparison of inductor volt-second with different C_n

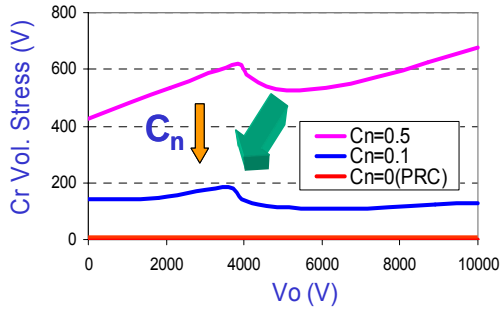

(c) Comparison of voltage stress on series resonant capacitor with different C_n

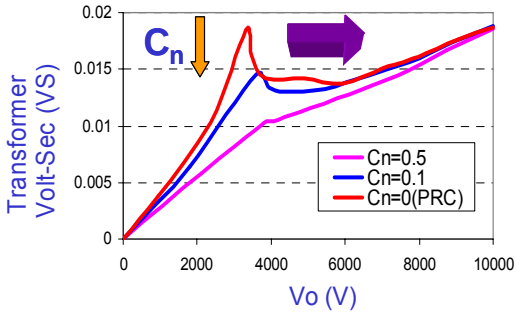

(d) Comparison of transformer volt-second with different C_n

Fig. 4.32. Design comparison for PRC, $C_n = 0.1$ and $C_n = 0.5$

As expected, the PRC ($C_n = 0$) has the best performance of the all designs. The inductor volt-second of PRC is the lowest of these three designs. This means that the volume of the resonant inductor will be significantly reduced. Meanwhile, the device loss of PRC remains low when compared with the other two designs. The volt-second of the transformer still stays almost the same for all three cases. Last, a considerable improvement of PRC is the reduction of resonant elements from three to two, which means the series resonant capacitor can be saved without hurting the performance of the

resonant converter. With these minor or major improvements, PRC will prove to be the optimum design after the entire investigation.

Finally, two designs are compared to show the improvement. The first one is an LCC resonant converter design based on the CCCP control method. The second one is the PRC with the CCCPF control scheme. Their circuit parameters are shown in Table 4-5.

Table 4-5. Circuit parameters for LCC and PRC converter with different control schemes

Control Mode	CCCPF	CCCP
C_n	0 (PRC)	0.5
M at 10 kV	3	2.6
Q at 10 kV	4	2.5
L_r (Prim.-side)	40.8 μH	62.4 μH
C_p (Prim.-side)	13.3 nF	15.0 nF
C_r (Prim.-side)	/	30.0 nF
Z_o	55.4 Ω	79.0 Ω
f_o	215.7 kHz	202 kHz
N_p:N_s	1:11	1:13
f_s Range	80~200 kHz	149~200 kHz

The performance of the two designs based on different control schemes is shown in Fig. 4.33.

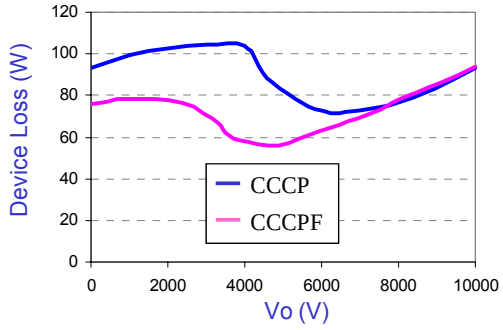

(a) Comparison of device loss with different control methods

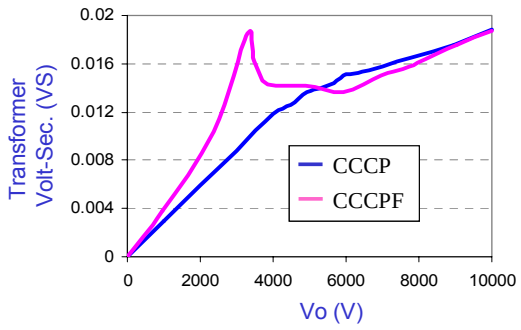

(b) Comparison of transformer volt-second with different control methods

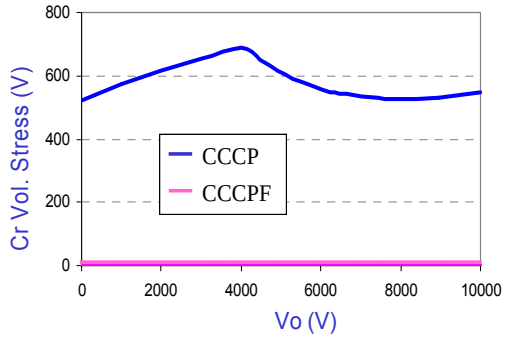

(c) Comparison of voltage stress on series resonant capacitor with different control methods

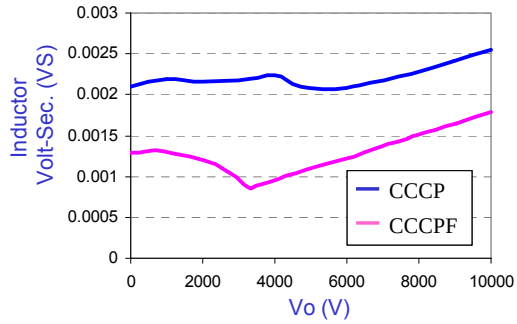

(d) Comparison of inductor volt-second with different control methods

Fig. 4.33. Design comparison for resonant converters with different control methods

Needless to say, the performance of the parallel resonant converter is much improved when compared with LCC converter. The control is the key to accomplish such improvement. As a result, the parallel resonant converter with the new CCCPF control is adopted as the final optimum design.

4.3.4 Control Implementation and Design Result

The parallel resonant converter is controlled by changing the switching frequency. The charging trajectory of the converter is illustrated in Fig. 4.31. Because the

switching frequency is relative to the output voltage, the output voltage can be used to control the operating frequency. Due to the variation of operation points, it is very difficult to provide the precise analytical solution of the control. Numeric solutions are applied to implement the variable switching frequency control. The relationship between output voltage and operation frequency is shown in Fig. 4.34.

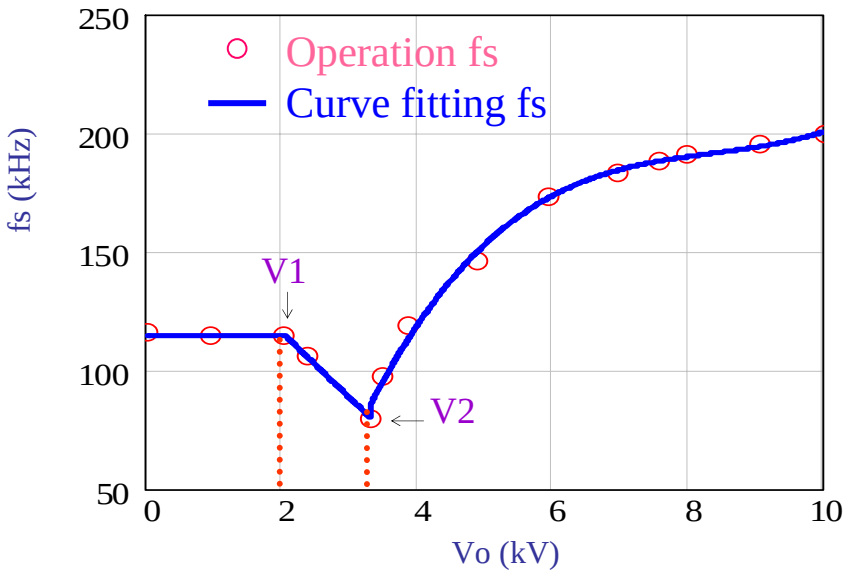

Fig. 4.34. Curve fitting results for the relationship between the operating frequency and the output voltage

The curve fitting result is shown below:

$$f_s = \begin{cases} a & (V_o \le V1) \\ b \cdot V_o + c & (V1 < V_o \le V2) \\ d \cdot V_o^3 + e \cdot V_o^2 + f \cdot V_o + g & (V_o \ge V2) \end{cases}$$

a	*b*	*c*	*d*	*e*	*f*	*g*
115	*171*	*-27.5*	*-233*	*145*	*17*	*0.7*

Both digital control and analog control can implement the control function. In Fig. 4.35, the control schematic is shown. The conventional analog control circuit could be easily designed based on this control schematic. To achieve variable frequency control, instead of a PWM comparator in a PWM controller, a Voltage Controlled Oscillator (VCO) is used to convert control voltage Vo to the variable frequency square wave, which is used to drive the switches.

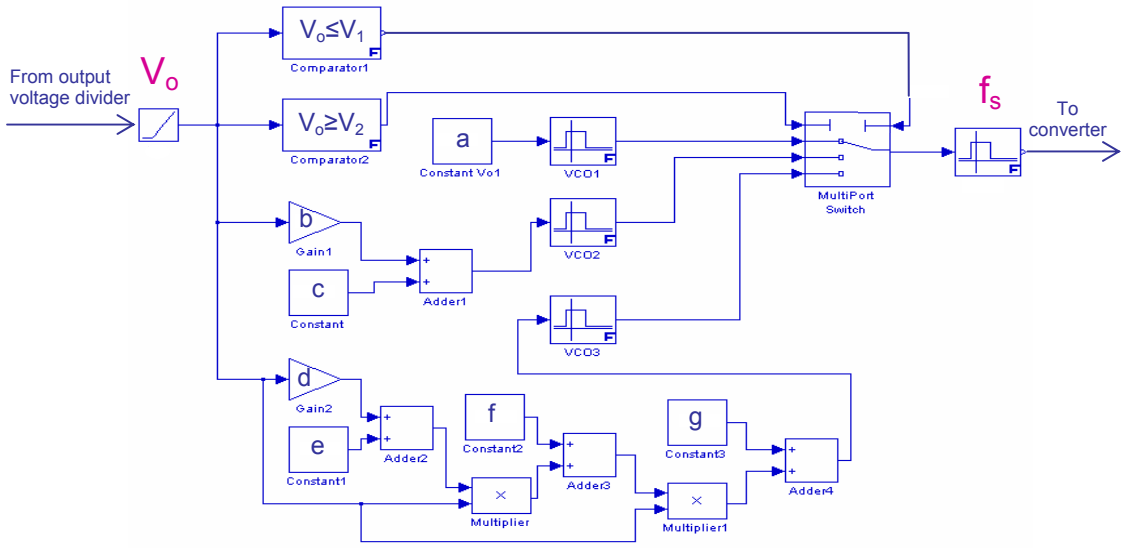

Fig. 4.35. The variable switching frequency control schematic of the parallel resonant converter

The operation of the PRC is demonstrated by simulation in SABER. In Fig. 4.36, it is demonstrated that the PRC can achieve the goal very well with the CCCPF control method.

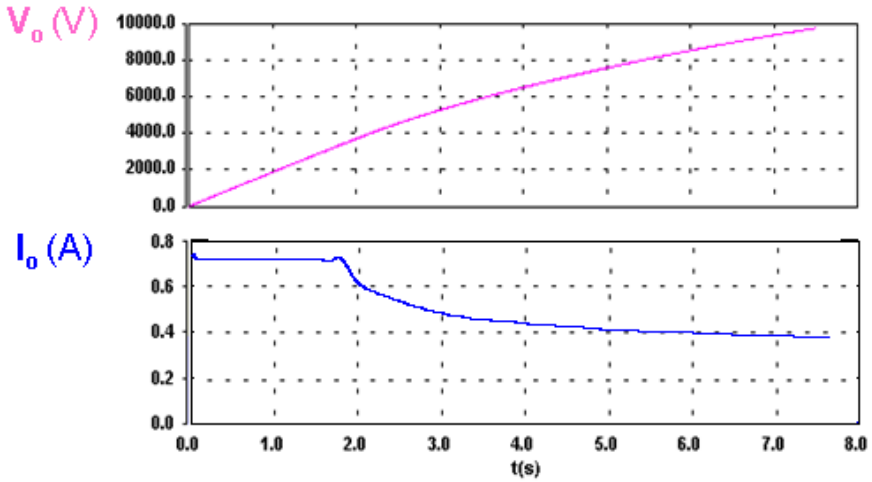

Fig. 4.36. Load capacitor charging waveforms with PRC by simulation. The upper trace: output voltage of the load capacitor; the lower trace: output current of the load capacitor

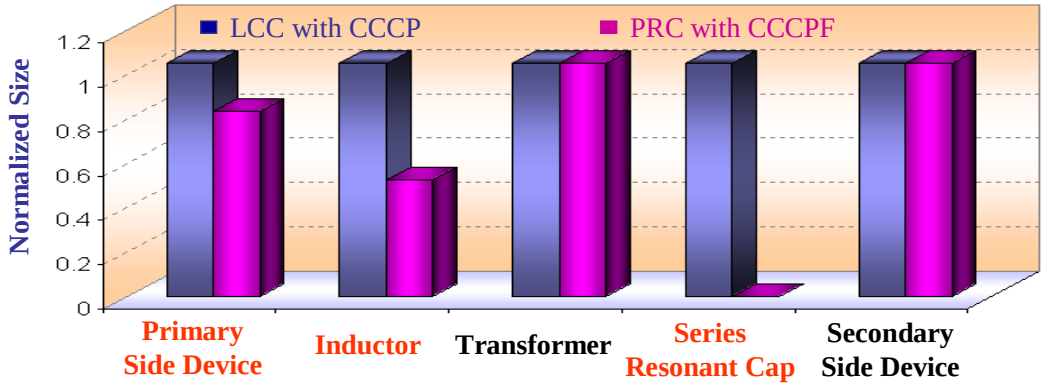

Fig. 4.37. Components volume comparison for resonant converters with different control methods

Volumes of the major components for different designs are compared in Fig. 4.37. It should be noted that the normalized size is applied to the comparison. Also, the normalized loss comparisons of the major components are illustrated in Fig. 4.38.

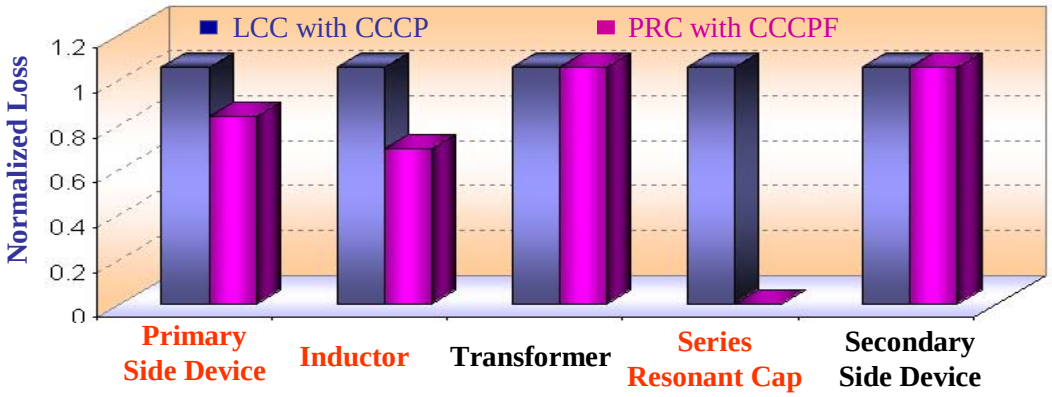

Fig. 4.38. Components loss comparison for resonant converters with different control methods

The prototype dimensions of different designs are shown in Fig. 4.39. The size of the LCC converter is $11.2in.\times 4.2in.\times 2.2in.$ (length:width:height). With a charging rate of 2.6kJ/S, the power density of the LCC converter is 25W/inch^3. For the parallel resonant converter, the size will be reduced to $9.8in.\times 3.9in.\times 2.2in.$. With the same load capacitor charging rate, the power density will increase to 31W/inch^3.

4.4 Summary

In this chapter, optimal designs of resonant converters have been thoroughly studied for high-voltage pulsed power application. The target has been to design the resonant converter, which could be optimized for the requirement of high efficiency and high power density.

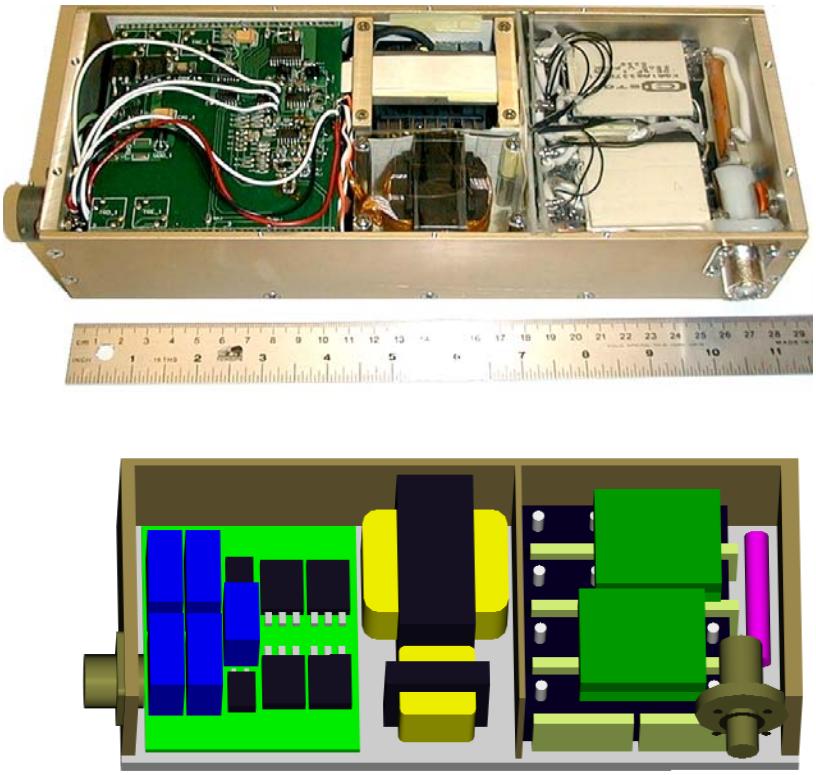

Fig. 4.39. Prototype dimensions comparison for different designs. The upper prototype: the LCC converter with CCCP control; the lower prototype: the PRC converter with CCCPF control

A novel constant power factor control is proposed. With the new CCCPF control scheme, the efficiency of the resonant converter will be effectively improved. With optimal selection of resonant tank values, the passive components size will be reduced. The parallel resonant converter is proved to be the most suitable topology for this application. The optimum design is provided, and the power density of 31W/inch^3 will be achieved.

Chapter 5

Summary and Future Work

5.1 Summary

Pulsed power technologies are widely used for X-ray generators, lithography, brilliant flashes of light and newly developed HDTV. The core of any pulsed power application is a high power density, low weight and efficient electric energy producer—pulsed power supply. One of the requirements for the next generation of pulsed power supplies is to achieve high power density with high efficiency.

Non-isolation type topologies have been used in this application. Due to the high voltage stress of the output, series-connected devices are inevitable. This will lead to slow switching transience and very low switching frequency. A multilevel boost converter is proposed to reduce the voltage stress of the devices. However, due to its complex structure, a multilevel boost converter suffers large passive components size.

A phase shift full-bridge PWM converter can achieve ZVS operation and reduce the switching loss. However, high-voltage transformer nonidealities will degrade the performance of this converter. Large voltage regulation range will exacerbate the

problem of circulating energy. Also, secondary diodes reverse recovery will be a severe problem for PWM techniques.

Resonant converters are well-known for their low switching loss. PRC and LCC resonant converters can fully utilize the high voltage transformer nonidealities and have full power control range with a small variation in frequency. Therefore, PRC and LCC are considered good candidates for pulsed power systems. With the help of the three-level structure, the low-voltage MOSFET can be used. The switching frequency can be increased to 200 kHz.

The power factor concept for the resonant converter is proposed and studied. Based on this concept, a new methodology to indicate the performance of the resonant converter is proposed and explored. The main idea is to optimize the resonant converter to operate in the high-power factor mode.

In order to increase the efficiency and power density of the converter, a new constant-power factor control is proposed and investigated. By applying this control scheme, the efficiency of the resonant converter will be much increased. By reducing the ratio of resonant capacitance of LCC, the passive components size will be shrunk. Finally, PRC is proven to be the optimum topology for the pulsed power application due to its high efficiency and small passive components size.

Based on the new CCCPF control, the power density of the parallel resonant converter can be achieved as high as 31 W/inch^3 with natural cooling.

5.2 Future work

As this thesis is proposed, the prototype of PRC with the new CCCPF control is being built. All the design results will be verified by the experiments in the future.

With the new constant power factor control, the MOSFETs' loss could be minimized. This gives us opportunity to push the pulsed power supplies to higher switching frequency. Therefore, the passive components size could be reduced. The high-voltage diodes' reverse recovery loss could be reduced if the high voltage Silicon Carbide (SiC) diodes are provided commercially in the near future.

In this work, the new constant power factor control is proposed. Following the control trajectory, the performance of the resonant converter should be very good. However, it is a kind of open-loop control. For capacitor-charging applications, the precise control is not so critical because no strict regulation process is required. But if used for the other applications, the precise control is needed. The study of closed-loop control is necessary. It is needed to develop the small-signal circuit model for this topology to complete the closed-loop control

Reference

A. Pulsed power and capacitor charging power supply

[A-1] M. Kristiansen, "Pulsed power applications," *Proc. Pulsed Power Conference*, 1993, vol.1, 21-23 Jun 1993, pp. 6-10.

[A-2] M. Gundersen, J. Dickens and W. Nunnally, "Compact, portable pulsed power: physics and applications," *Proc. Pulsed Power Conference,* 2003, vol.1, 15-18 June, 2003, pp.9-12.

[A-3] G. J. Rohwein, R. N. Lawson and M. C. Clark, "A compact 200kV pulse transformer system," *Proc. Pulsed Power Conference*, 1991, pp. 968-970.

[A-4] M. Buttram, "Some future directions for repetitive pulsed power," *IEEE Trans. on Plasma Science*, 2002 pp. 262-266.

[A-5] M.A. Kempkes, J.A. Casey, M.P.J. Gaudreau, T.A. Hawkey and I.S. Roth, "Solid-state modulators for commercial pulsed power systems," *Proc. Power Modulator Symposium*, 2002, pp. 689-693.

[A-6] Y.S. Jin, H.S. Lee, J.S. Kim, Y.B. Kim and G.H. Rim, "Compact 200kJ pulse power system with a simple crowbar circuit," *Proc. Pulsed Power Conference*, 2003, pp. 1239 - 1242.

[A-7] B.E. Strickland, M. Garbi, F. Cathell, S. Eckhouse and M. Nelms, "2 kJ/s, 25 kV high frequency capacitor charging power supply using MOSFET switches," *Proc. Power Modulator Symposium*, 1990, pp. 531-534.

[A-8] R.M. Nelms and J.E. Schatz, "A capacitor charging power supply utilizing a Ward converter," *IEEE Trans. on Industrial Electronics*, 1992, pp. 421-428.

[A-9] M. Giesselmann and T. Heeren, "Rapid capacitor charger," *Proc. Power Modulator Symposium*, 2002, pp. 146-149.

[A-10] M. Giesselmann and E. Kristiansen, "Design of a 30 kV power supply for rapid capacitor charging," *Proc. Power Modulator Symposium,* 2000, pp. 115-118.

[A-11] H. Pollock, "High efficiency, high frequency power supplies for capacitor and battery charging" *IEE Proc. Power Electronics for Demanding Applications*, 1999, pp. 901-910.

[A-12] B.E.F. Cathell, S. Pronko, S. Eckhouse and N. Nelms, "8 kJ/s high frequency capacitor charging power supply using parallel inverters," *Proc. Pulsed Power Conference,* 1995, pp. 245-248.

B. Topologies for capacitor charging power supply

[B-1] P.K. Bhadani, "Capacitor-charging power supply for laser pulsers using a boost converter," *Rev. Sci. Instrum.*, 1989, pp. 605-607.

[B-2] B. Axelrod, Y. Berkovich and A. Ioinovici, "Transformerless DC-DC converters with a very high DC line-to-load voltage ratio," *Proc. Int. Sym. on Circuits and Systems (ISCAS)*, 2003, vol.3, pp. 435-438.

[B-3] O. Abutbul, A. Gherlitz, Y. Berkovich and A. Ioinovici, "Boost converter with high voltage gain using a switched capacitor circuit," *Proc. ISCAS*, 2003, vol.3, pp. 296-299.

[B-4] L. Huber and M. M. Jovanovic, "A design approach for server power supplies for networking," *Proc. IEEE Applied Power Electronics Conf. (APEC)*, 2000, vol.2, pp. 1163-1169.

[B-5] H. Wu and X. He, "Single phase three-level power factor correction circuit with passive lossless snubber," *IEEE Trans. on Power Electronics*, Nov. 2002, vol.17, pp. 946-953.

[B-6] B. Lin, Y. Hou and H. Chiang, "Implementation of a three-level rectifier for power factor correction," *IEEE Trans. on Power Electronics*, Sept. 2000, vol.15, pp. 891-900.

[B-7] M.T. Zhang, Y. Jiang, F.C. Lee and M.M. Jovanovic, "Single-phase three-level boost power factor correction converter," *Proc. APEC*, 1995, vol.1, pp. 434-439.

[B-8] W. Chen, F.C. Lee, M.M. Jovanovic, J.A. Sabate, "A Comparative Study Of A Class Of Full Bridge Zero Voltage Switched PWM Converters," *Proc. APEC,* 1995, pp. 893-899.

[B-9] A.W. Lotfi, Q. Chen, F.C. Lee, "A Nonlinear Optimization Tool For The Full Bridge Zero Voltage Switched DC-DC Converter," *Proc. IEEE Power Electronics Specialists Conf (PESC),* 1992, pp. 1301-1309.

[B-10] Xinbo Ruan; Yangguang Yan, "Soft-Switching Techniques For PWM Full Bridge Converters," *Proc. PESC,* 2000, vol.2, pp. 634 -639.

[B-11] D.B. Dalal, F.S. Tsai, "A 48V, 1.5kw, Front-End Zero Voltage Switches PWM Converter With Lossless Active Snubbers For Output Rectifiers," *Proc. APEC,* 1993, pp. 722-728.

[B-12] J.G. Cho, J.A. Sabate, G. Hua, and F.C. Lee, "Zero Voltage And Zero Current Switching Full Bridge PWM Converter For High Power Applications," *Proc. PESC*, 1994.

[B-13] B.H., Choo; D.Y., Lee; S.B. Yoo and D.S. Hyun, "A novel full-bridge ZVZCS PWM DC/DC converter with a secondary clamping circuit," *Proc. PESC*, 1998, pp. 936-941.

[B-14] B.H., Choo; B.K., Lee; S.B. Yoo and D.S. Hyun, "A novel secondary clamping circuit topology for soft switching full-bridge PWM DC/DC converter," *Proc. APEC*, 1998, pp. 840-845.

[B-15] S. Valtchev, B.V. Borges, "Improved full bridge zero voltage switched phase shift DC/DC converter using a secondary clamped inductor," *Proc. Industrial Electronics, Control and Instrumentation Conf. (IECON)*, 1995, pp. 258-264.

[B-16] W.G. Homeyer, R.J. Callanan, E.E. Bowles and A. Nerem, "1.2 MW DC-DC converter," *IEEE Trans. on Magnectics*, 1993, pp. 992-996.

[B-17] J. Biebach, P. Ehrhart, A. Muller, G. Reiner and W. Weck, "Compact modular power supplies for superconducting inductive storage and for capacitor charging," *IEEE Trans. on Magnectics*, 2001, pp. 353-357.

[B-18] B.E. Strickland, M. Garbi, F. Cathell, S. Eckhouse and M. Nelms, "2 kJ/s, 25 kV high frequency capacitor charging power supply using MOSFET switches," *Proc. Power Modulator Symposium*, 1990, pp. 531-534.

[B-19] M. Souda, F. Endo, C. Yamazaki, K Okamura and K. Fukushima, "Development of high power capacitor charging power supply for pulsed power applications," *Proc. Pulsed Power Conf.*, 1999, pp. 1414-1416.

[B-20] A.C. Lippincott, R.M. Nelms, M. Garbi and E. Strickland, "A series resonant converter with constant on-time control for capacitor charging applications," *Proc. APEC*, 1990, pp. 147-154.

[B-21] H. Pollock and J.O. Flower, "Design, simulation and testing of a series resonant converter for pulsed load applications," *Proc. Power Electronics and Variable-Speed Drives*, 1994, pp. 256-261.

[B-22] F. Canales, P. Barbosa and F.C. Lee, "A zero-voltage and zero-current switching three-level DC/DC converter," *IEEE Trans. on Power Electronics*, 2002, pp. 898-904.

[B-23] Y. Gu and Z. Qian, "Three level LLC series resonant DC/DC converter," *Proc. APEC*, 2004, pp. 1647-1652.

[B-24] J.R. Pinheiro and I. Barbi, "Three-level zero-voltage-switching PWM DC-DC converters-a comparison," *Proc. PESC*, 1995, pp. 914-919.

[B-25] B.J. Baliga, "Power semiconductor device figure of merit for high-frequency applications," *IEEE, Electron Device Letters*, 1989, pp. 455–457.

[B-26] I. Kim; S. Matsumoto, T. Sakai and T. Yachi, "New power device figure of merit for high-frequency applications," *Proc. Power Semiconductor Devices and ICs*, 1995, pp. 309-314.

[B-27] C. Rexer, Fairchild Semiconductor, "Advancements in power semiconductor solutions," *IEEE, APEC, Special Presentation Sessions*, 2004.

C. Resonant converter and power factor

[C-1] A. Witulski, "Steady state analysis and design of the series resonant converter," *M.S. thesis*, University of Colorada, Mar. 1986.

[C-2] G. Ivensky, A. Kats and S.Ben-Yaakov, "An RC load model of parallel and series-parallel resonant DC-DC converters," *IEEE Trans. on Power Electronics*, 1999, pp. 515-521.

[C-3] R. Oruganti, J. Yang, and F.C. Lee, "Implementation of Optimal Trajectory Control of Series Resonant Converters," *Proc. IEEE PESC,* 1987.

[C-4] A.K.S. Bhat, "Analysis and Design of a Modified Series Resonant Converter," *IEEE Trans. on Power Electronics*, 1993, pp. 423-430.

[C-5] J.T. Yang and F.C. Lee, "Computer Aided Design and Analysis of Series Resonant Converters," *Proc. IEEE IAS,* 1987.

[C-6] V. Vorperian and S. Cuk, "A Complete DC Analysis of the Series Resonant Converter," *Proc. IEEE PESC, 1*982.

[C-7] R. Oruganti, J. Yang, and F.C. Lee, "State Plane Analysis of Parallel Resonant Converters," *Proc. IEEE PESC*, 1985.

[C-8] R. Liu, I. Batarseh, C.Q. Lee, "Comparison of Capacitively and Inductively Coupled Parallel Resonant Converters," *IEEE Trans. on Power Electronics*, 1993, vol.8, pp. 445-454.

[C-9] M. Emsermann, "An Approximate Steady State and Small Signal Analysis of the Parallel Resonant Converter Running Above Resonance," *Proc. Power Electronics and Variable Speed Drives*, 1991, pp. 9-14.

[C-10] Y.G. Kang, A.K. Upadhyay, D. Stephens, "Analysis and Design of a Half Bridge Parallel Resonant Converter Operating Above Resonance," *Proc. IEEE IAS*, 1998, pp. 827-836.

[C-11] Robert L. Steigerwald, "A Comparison of Half Bridge Resonant Converter Topologies," *IEEE Trans. on Power Electronics*, 1988, pp. 174-182.

[C-12] R. Oruganti and F.C. Lee, "Resonant Power Processors, Part 2: Methods of Control," *IEEE Trans. on Industrial Application*, 1985.

[C-13] R. Severns, "Topologies For Three Element Resonant Converters," Proc. IEEE APEC '90, 1990, pp. 712-722.

[C-14] Vatche Vorperian, "Analysis Of Resonant Converters," Dissertation, California Institute of Technology, 1984.

[C-15] K.H. Liu, "Resonant Switches Topologies and Characteristics," *Proc. IEEE PESC*, 1985, pp. 106-116.

[C-16] M. Zaki, A. Bonsall, I. Batarseh, "Performance Characteristics for the Series Parallel Resonant Converter," *Proc. Southcon*, 1994, pp.573-577.

[C-17] A.K.S. Bhat, "Analysis, Optimization and Design of a Series Parallel Resonant Converter," *Proc. IEEE APEC*, 1990, pp. 155-164.

[C-18] A.K.S. Bhat, "Analysis and Design of a Series Parallel Resonant Converter With Capacitive Output Filter," *Proc. IEEE IAS*, 1990, pp. 1308-1314.

[C-19] R. Liu, and C.Q. Lee, "Series Resonant Converter with Third-Order Commutation Network," *IEEE Trans. on Power Electronics*, 1992, pp. 462-467, vol.7, issue 3.

[C-20] J.F. Lazar, R. Martinelli, "Steady State Analysis of the LLC Series Resonant Converter," *Proc. IEEE APEC*, 2001, pp.728-735.

[C-21] R. Elferich, T. Duerbaum, "A New Load Resonant Dual Output Converter," *Proc. IEEE PESC*, 2002, pp.1319-1324.

[C-22] B. Yang, F.C. Lee, A.J. Zhang and G. Huang, "LLC Resonant Converter For Front End DC/DC Conversion," *Proc. IEEE APEC,* 2002, pp. 1108-1112 vol.2.

[C-23] R. Farrington, M.M. Jovanovic, and F.C. Lee, "Analysis of Reactive Power in Resonant Converters," *Proc. IEEE PESC*, 1992.

[C-24] R. Farrington, M.M. Jovanovic, and F.C. Lee, "Design oriented analysis of reactive power in resonant converters," *IEEE Trans. on Power Electronics*, 1993, pp. 411-422.

[C-25] J.B. Klaassens, M.P.N. van Wesenbeeck and H.K. Lauw, "Series-resonant single-phase AC-DC power supply with control of reactive power," *IEEE Trans. on Power Electronics*, 1992, pp. 111-118.

[C-26] A.L. Melse and S.W.H. de Haan, "Reactive power handling with series-resonant converters," *IEEE Trans. on Power Electronics*, 1988, pp. 17-25.

[C-27] N. Balabanian, "Fundamentals of circuit theory," *Textbook, Allyn and Bacon*, 1961

[C-28] W. Shepherd and P. Zand, "Energy Flow and Power Factor in Nonsinusoidal Circuits," *Textbook, Cambridge University Press*, 1979

[C-29] R. W. Erickson and D. Maksimovic, "Fundamentals of Power Electronics," *Textbook, Kluwer Academic Publishers*, 2nd. Edition, 2001.

[C-30] J. A. Sabete, "Zero-voltage switched resonant and PWM converters: design-oriented analysis and performance evaluation," *Ph.D Dissertation, Virginia Tech*, 1994.

[C-31] R. Elwell, J, Cherry and S. Fagan, "Current and voltage controlled capacitor charging schemes," *IEEE Trans. on Magnetics*, 1995, pp. 38-42

D. Others

[D-1] P.E. Bagnoli, C. Casarosa, M. Ciampi, E. Dallago, "Thermal resistance analysis by induced transient (TRAIT) method for power electronic devices thermal characterization. I. Fundamentals and theory," *IEEE Trans. on Power Electronics*, 1998, pp. 1208-1219.

[D-2] L.-T Yeh and R.C. Chu, "Thermal Management of Microelectronic Equipment," *Textbook*, *New York: ASME Press*, 2002.

[D-3] F.P. Incropera and D.P. DeWitt, "Fundamentals of heat and mass transfer," *Textbook*, *New York: John Wiley & Sons, Inc.*, 2002.

[D-4] W.H. Tang, Q.H. Wu and Z.J. Richardson, "A Simplified Transformer Thermal Model Based on Thermal-Electric Analogy," *IEEE Trans. on Power Delivery*, 2004, pp. 1112–1119.

[D-5] G. Swift, T.S. Molinski and W. Lehn, "A fundamental approach to transformer thermal modeling. I. Theory and equivalent circuit," *IEEE Trans. on Power Delivery*, 2001, pp. 171-175.

[D-6] G. Swift and T.S. Molinski, "A fundamental approach to transformer thermal modeling. II. Field verification," *IEEE Trans. on Power Delivery*, 2001, pp. 176-180.

Vita

Dianbo Fu

The author was born in Changsha, Hunan, China in 1978. He received the Bachelor of Science degree in Electrical Engineering from Huazhong University of Science and Technology, Wuhan, China, in 2001.

Since August 2002, he has been working towards the Master of Science degree at the Bradley Department of Electrical and Computer Engineering, Virginia Polytechnic Institute and State University. Working as a research assistant at the Center for Power Electronics Systems, his research interests include high-frequency power factor correction (PFC) converters design and high-frequency DC/DC converters design.